Received: 19 August 2020 | Revised: 24 October 2020 | Accepted: 5 November 2020

DOI: 10.1111/pce.13955

ORIGINAL ARTICLE

Plant, Cell & Environment WILEY

Ethylene is a local modulator of jasmonate-dependent phenolamide accumulation during *Manduca sexta* herbivory in *Nicotiana attenuata*

Florent Figon[1,2] | Ian T. Baldwin[1] | Emmanuel Gaquerel[1,3]

[1]Department of Molecular Ecology, Max Planck Institute for Chemical Ecology, Jena, Germany

[2]Master BioSciences, ENS de Lyon, UCB Lyon 1, Université de Lyon, Lyon, France

[3]Institut de Biologie Moléculaire des Plantes du CNRS, Université de Strasbourg, Strasbourg, France

Correspondence
Emmanuel Gaquerel, Institut de Biologie Moléculaire des Plantes du CNRS, Université de Strasbourg, Strasbourg, France.
Email: emmanuel.gaquerel@ibmp-cnrs.unistra.fr

Present address
Florent Figon, Institut de Recherche sur la Biologie de l'Insecte, UMR 7261, CNRS, Université de Tours, Tours, France.
Email: florent.figon@univ-tours.fr

Funding information
Collaborative Research Centre 'Chemical Mediators in Complex Biosystems - ChemBioSys' (SFB 1127) from the DFG

Abstract

Rapid reconfigurations of interconnected phytohormone signalling networks allow plants to tune their physiology to constantly varying ecological conditions. During insect herbivory, most of the induced changes in defence-related leaf metabolites are controlled by jasmonate (JA) signalling, which, in the wild tobacco *Nicotiana attenuata*, recruits MYB8, a transcription factor controlling the accumulation of phenolic-polyamine conjugates (phenolamides). In this and other plant species, herbivory also locally triggers ethylene (ET) production but the outcome of the JA-ET cross-talk at the level of secondary metabolism regulation has remained only superficially investigated. Here, we analysed local and systemic herbivory-induced changes by mass spectrometry-based metabolomics in leaves of transgenic plants impaired in JA, ET and MYB8 signalling. Parsing deregulations in this factorial data-set identified a network of JA/MYB8-dependent phenolamides for which impairment of ET signalling attenuated their accumulation only in locally damaged leaves. Further experiments revealed that ET, albeit biochemically interrelated to polyamine metabolism via the intermediate *S*-adenosylmethionine, does not alter the free polyamine levels, but instead significantly modulates phenolamide levels with marginal modulations of transcript levels. The work identifies ET as a local modulator of phenolamide accumulations and provides a metabolomics data-platform with which to mine associations among herbivory-induced signalling and specialized metabolites in *N. attenuata*.

KEYWORDS
ethylene signalling, jasmonate signalling, metabolomics, phenolamides, plant–insect interactions

1 | INTRODUCTION

Plants, as sessile organisms, must continuously adjust their physiology to cope with fluctuating abiotic and biotic conditions. To resist insect herbivory, plants have evolved efficient constitutive as well as inducible defence strategies, the latter being thought to mitigate resource allocation costs to defence during a plant's ontogeny (Heil & Baldwin, 2002). Defence induction translates from the activation and complex interactions among phytohormone signal transduction pathways, which are triggered in attacked and distant leaves in response to insect feeding (Erb, Meldau, & Howe, 2012).

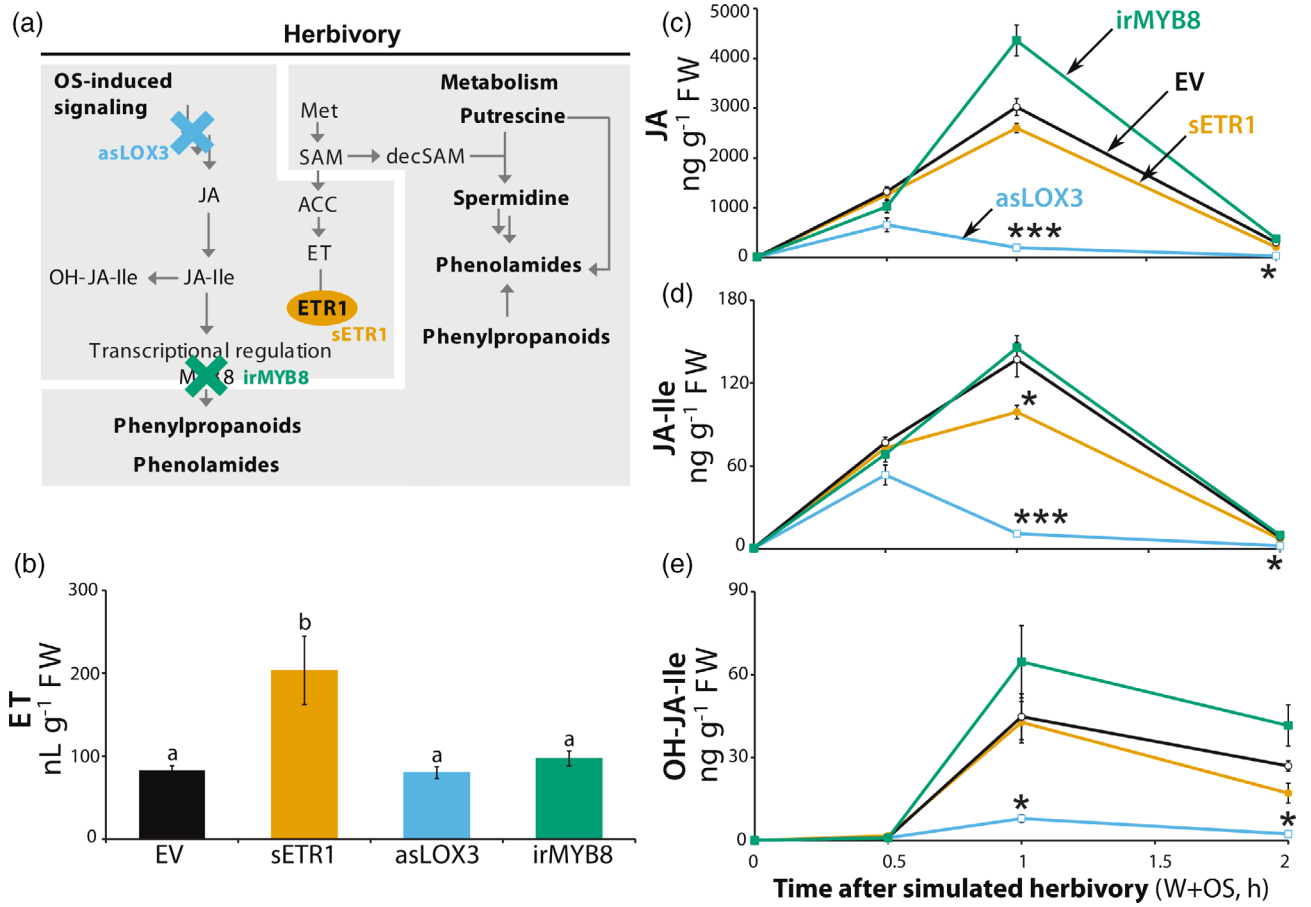

FIGURE 1 Genetic manipulations of herbivory-induced jasmonate and ethylene accumulation in leaves of *N. attenuata*. (a) Simulated leaf herbivory by *M. sexta* herbivory elicits the production of ethylene (ET) and jasmonates in *N. attenuata* and dependent signalling and metabolic reconfigurations. Three different *N. attenuata* transgenic lines were used for studying interactions between these hormonal pathways: (i) an asLOX3 line in which the first oxidative step for jasmonate biosynthesis is impaired, (ii) an sETR1 line expressing a non-functional mutated version of ETR1, the ET receptor and (iii) an irMYB8 line with silenced transcripts for MYB8, the core JA-dependent transcription factor controlling gene expression for defensive phenylpropanoid-polyamine conjugates (phenolamides) accumulation. Ethylene synthesis requires*S*-adenosylmethionine (SAM), whose decarboxylated form (decSAM, decarboxylated-*S*-adenosylmethionine) is required within the polyamine biosynthetic pathway. (b) Mean levels (±*SE*, five biological replicates) of ET emission produced from leaf discs of the different genotypes accumulated over 10 hr after simulated herbivory by mechanical wounding and application of *M. sexta* oral secretions (W + OS). Different letters indicate significant differences ($p \leq .05$, ANOVA followed by Tukey HSD post hoc tests) between genotypes. (c–e) Mean levels (±*SE*, five biological replicates) of JA, JA-Ile and OH-JA-Ile in leaves elicited by W + OS treatment. Asterisks indicate significant differences compared to an empty vector (EV) control at specific time points (*$p \leq .05$, ***$p \leq .001$, one-way ANOVA followed by Tukey HSD post hoc tests; when normality assumption was not met, Kruskal–Wallis and pairwise Wilcoxon rank sum tests were applied). ACC, 1-aminocyclopropane-1-carboxylic acid; decSAM, decarboxylated-*S*-adenosylmethionine; JA-Ile, JA-Isoleucine; Met, methionine; OH-JA-Ile, hydroxy-JA-Ile

Activation of ethylene (ET) signalling is part of the hormonal response of plants against attackers. ET biosynthesis involves the two-step transformation of *S*-adenosylmethionine (SAM) into ET by ACS [1-Aminocyclopropane-1-Carboxylate (ACC) Synthase] and ACO (ACC oxidase) (Figure 1a). The interaction between ET and the ETR1 receptor protein, leads to the activation of ET-dependent transcriptional responses (Figure 1a; Stepanova & Alonso, 2009). This signalling pathway is known to contribute to the regulation of induced defences in the wild tobacco *Nicotiana attenuata* after attack by the specialized larvae of *Manduca sexta* (Onkokesung, Galis, et al., 2010; von Dahl et al., 2007). Conversely, the performance of this herbivore is strongly improved when feeding on *N. attenuata* lines deficient in ET signalling (Onkokesung, Baldwin, & Gális, 2010). In cultivated tobacco in addition to *N. attenuata*, ET signalling is well-known to antagonize the jasmonate-dependent accumulation of the defensive neurotoxin, nicotine (Winz & Baldwin, 2001). This regulatory response is thought to function as a means of adjusting nitrogen investments into costly nicotine production and requires several ERF (Ethylene Response Factor) transcription factors part of the NIC regulatory loci positively controlling nicotine biosynthetic genes (Shoji, Kajikawa, & Hashimoto, 2010). *M. sexta* larvae are known to be tolerant of high nicotine levels (Snyder, Walding, & Feyereisen, 1994). Hence, the important increases in *M. sexta* performance that were previously detected when feeding on ET signalling deficient plants likely translate from more profound and yet-to-be-explored deregulations of the host plant defence metabolism. In this respect, cross-talks between ET and other

herbivory-induced hormonal sectors have been characterized at the molecular level (Wang, Li, & Ecker, 2002) and are likely to account for the deregulated defence response in *N. attenuata* lines rendered genetically insensitive to ET perception (Li, Halitschke, Baldwin, & Gaquerel, 2020; von Dahl et al., 2007).

Jasmonate signalling exerts a central regulatory function for most of the transcriptional changes and metabolic reconfigurations contributing to induced responses to insect herbivory (Wasternack & Hause, 2013). In *N. attenuata*, *M. sexta* feeding elicits a rapid burst of all jasmonate biosynthetic intermediates, leading to transient and herbivory-specific accumulations of both jasmonic acid (JA) and its bioactive conjugate JA-Isoleucine (JA-Ile) (Kallenbach, Alagna, Baldwin, & Bonaventure, 2010; Paschold, Bonaventure, Kant, & Baldwin, 2008). A large body of research on this ecological interaction has shown that JA-Ile signalling is critical for the efficient activation of an anti-herbivore arsenal (reviewed in Wang & Wu, 2013), which includes the above-mentioned nicotine, trypsin proteinase inhibitors acting as anti-digestive proteins (Kang, Wang, Giri, & Baldwin, 2006), as well as a broad set of phenolamides whose contribution to anti-herbivore defences was more recently uncovered (Onkokesung et al., 2011). Several studies have reported convergent evidence for a key role played by the interplay between JA and ET signalling pathways in the adjustment of appropriate defence investments to different caterpillar species (reviewed in Erb et al., 2012). In addition to the well-characterized function of ET in tuning the JA-induced nicotine production, its regulatory role over other classes of defence metabolites remains poorly examined. In the case of phenolamides, a recent large-scale metabolomics study, which tested predictions of seminal hypotheses on the remodelling of specialized metabolite production during insect herbivory, has revealed that ET signalling finely tunes the metabolic responses of different *Nicotiana* species according to the herbivore species (Li et al., 2020).

Phenolamides, which result from the conjugation of hydroxycinnamic units to a polyamine skeleton (Figure 1a), are important constitutively produced and/or stress-inducible metabolites in the vegetative tissues of many plant species, including rice and *N. attenuata* (Alamgir et al., 2016; Onkokesung et al., 2011). In *N. attenuata*, the biosynthesis of these defensive specialized metabolites is strongly induced by the attack of *M. sexta*. One of these compounds, *N*-caffeoylputrescine, has been rigorously demonstrated to negatively affect *M. sexta* performance (Kaur, Heinzel, Schottner, Baldwin, & Galis, 2010). Similar to the well-characterized nicotine regulation, elevations in phenolamide levels also impart significant trade-offs for nitrogen allocation during insect herbivory and hence necessitates fine-tuning mechanisms, which remain largely unknown (Ullmann-Zeunert et al., 2013). From a biosynthetic standpoint, conjugation of CoA-activated hydroxycinnamic acid units onto polyamine skeletons translates from the enzymatic activities of a diverse array of BAHD *N*-acyltransferases, with AT1, DH29 and CV86 being the three BAHD controlling most of the phenolamide production in *N. attenuata* (Onkokesung et al., 2011). Briefly, AT1 has been shown to control the acylation of putrescine with coumaroyl-CoA or caffeoyl-CoA. DH29 was demonstrated to catalyse the first acylation step on spermidine, while CV86 is involved in the production of certain di-acylated spermidine isomers from DH29-dependent mono-acylated spermidines, suggesting that additional *N*-acyltransferases are likely required to produce the full spectrum of phenolamides found in *N. attenuata*. The expression of *AT1*, *DH29* and *CV86* is controlled by the transcription factor MYB8, a master regulator of phenolamide biosynthesis, as evidenced by the presence of MYB8 binding sites in the promoters of those genes (Schäfer et al., 2017) and by the fact that MYB8-deficient plants are virtually free of phenolamides (Kaur et al., 2010; Onkokesung et al., 2011).

Here, we test whether herbivory-induced ET signalling modulates the jasmonate- and MYB8-dependent production of defensive phenolamides in *N. attenuata* leaves attacked by *M. sexta*. To comprehensively examine interplay among JA and ET signalling sectors over herbivory-induced metabolic reconfigurations, we analysed local and systemic herbivory-induced changes in leaves of transgenic plants impaired in JA (asLOX3), ET (sETR1) and MYB8 (irMYB8) signalling using mass spectrometry-based metabolomics. The attack from *M. sexta* was simulated by the application of oral secretions (OS) from caterpillars on the leaves. From the exploration of metabolic class-specific deregulations in this factorial dataset, we detected that ET signalling is essential for the intact production of phenolamides in locally damaged leaves. Further, we examined whether a possible metabolic cross-talk, via the shared intermediate *S*-adenosylmethionine (SAM), between the production of ET and free polyamine metabolic homeostasis could have influence the channelling of putrescine and spermidine units for phenolamide production at the site of attack. Quantitative analyses of free polyamines and main phenolamides revealed that herbivory-induced ET biosynthesis does not destabilize polyamine homeostasis, but instead marginally affects transcript levels (*MYB8* and *CV86*) in this pathway. From these results, we infer that ET is a local regulator of defensive phenolamides during herbivory.

2 | MATERIALS AND METHODS

2.1 | Plant material

Selected transgenic lines with suppressed transcript levels for key genes in the herbivory-induced transduction cascade of *N. attenuata* were used in this study. An empty vector (EV) construct was used as control genetic background in most experiments. The phenotypic and molecular characterization of each of these lines has been previously published. Briefly, sense *ETR1* (*ETHYLENE RECEPTOR1*, sETR1) plants ectopically express a non-functional version of ETR1 (von Dahl et al., 2007). These plants are ethylene-insensitive and the negative feedback exerted by ethylene perception over its own production is disrupted, resulting in higher ethylene emissions after attack from *M. sexta* in this transgenic line (Figure 1b). Antisense *LOX3* (*LIPOXYGENASE3*, asLOX3) plants constitutively express a fragment of the *LOX3* gene in an antisense orientation, which leads to the silencing of endogenous *LOX3* transcripts by RNAi (Halitschke & Baldwin, 2003). asLOX3 plants are impaired in the first oxidation step within the JA biosynthetic pathway, thereby leading to a strong depletion of the herbivory-elicited jasmonate bursts. Inverted repeat *MYB8*

(irMYB8) plants constitutively express inverted repeat fragments of the *MYB8* gene, which results in the silencing of endogenous *MYB8* by RNAi (Kaur et al., 2010). Phenolamide biosynthesis, which is transcriptionally coordinated by the action of MYB8, is almost completely abolished in this transgenic line. The irACO transgenic line used in the experiment presented in Figure S3 exhibits constitutively repressed transcript levels for the ethylene biosynthesis gene *ACO* (*1-AMINOCYCLOPROPANE-1-CARBOXYLIC ACID OXIDASE*), thereby resulting in a strong impairment of ethylene production.

All seeds were first sterilized and incubated with diluted smoke and 0.1 M GA3, as previously described (Krügel, Lim, Gase, Halitschke, & Baldwin, 2002), and then germinated on plates containing Gamborg B5 medium. Ten-day-old seedlings were transferred to small pots (TEKU JP 3050 104 pots; Pöppelmann) with Klasmann plug soil (Klasmann-Deilmann), and after 10 days, seedlings were transferred to 1-L pots. Plants were grown in the glasshouse with a day/night cycle of 16 hr (26–28°C)/8 hr (22–24°C) under supplemental light from Master Sun-T PIA Agro 400 or Master Sun-TPIA Plus 600-W sodium lights (Philips Sun-T Agro). All experiments were conducted with 40 to 45-day old rosette-stage plants.

2.2 | Simulated herbivory treatment and experimental design

Oral secretions (OS) from third instar *M. sexta* larvae were collected with a pipette, pooled and kept under argon at −20°C until further use. At the start of the elicitation procedure, one source-sink transition leaf (youngest fully expanded leaf, referred as leaf position 0) from each plant was rapidly harvested, flash-frozen in liquid nitrogen and later used as pre-treatment controls. For each plant, two rosette leaves referred to as 'local' leaves (leaf positions +1 and + 2 in Figure 2a), were mechanically wounded with a fabric pattern wheel and 20 μL of 1/eighth water-diluted OS were directly applied on the wounds. This procedure hereafter referred to as 'W + OS elicitation' has been shown in previous studies to recapitulate a large proportion of the reconfigurations detected at the level of early signalling events, transcriptome and metabolome dynamics during direct *M. sexta* herbivory (Halitschke, Schittko, Pohnert, Boland, & Baldwin, 2001). Two younger sink leaves (leaf positions −1 and − 2 in Figure 2a) growing above locally treated leaves and with a minimal angular distance were collected as untreated 'systemic' leaves and pooled prior metabolite extraction.

In all experiments, five independent plants for each sampling time points were used resulting in five biological replicates. Briefly, samples for specialized metabolite profiling were harvested for both local and systemic leaf positions at 0 (control untreated transition leaf, see above), 24, 48 and 72 hr post-elicitation. The same experimental design was used for the harvest of local and systemic leaf samples to monitor dynamics of free polyamines, with the exception that additional sampling times (0.5, 1, 2, 4 and 6 hr) were considered to detect early changes to the W + OS treatment. Finally, to investigate changes in peaking levels of phytohormones across the different transgenic lines, only local leaves harvested 0, 0.5, 1, 1.5 and 2 hr after starting the elicitation were considered for analysis.

2.3 | Quantitative real-time PCR analysis

Total RNA from 100 mg of ground tissues was extracted as described by Linke et al. (2002). RNA was then treated with DNase using the DNA-free kit from Ambion following the manufacturer's protocol. cDNA synthesis was performed using the RevertAid H Minus Reverse Transcriptase from ThermoScientific and a poly-T primer according to the manufacturer's protocol. RT-qPCR was performed with a Stratagene MX3005P instrument. Transcript levels were calculated with a calibration curve of cDNA. For normalization, transcript levels of the housekeeping gene *ELF1α* were used (*EF1-α*, Acc. No. D63396). Untreated leaf controls harvested at the start of the elicitation procedure were used to examine basal transcript levels. To assess cross-genotype variations in W + OS-induced transcript levels, local leaves harvested 2 hr after elicitation were considered since a previous transcriptomics study has shown that the focal transcripts reached maximum levels for this time point. Primers are summarized in Table S1.

2.4 | Quantification of herbivory-induced ethylene emissions

Leaf discs were obtained from untreated plants for ethylene quantification. Directly after collection, these leaf discs were wounded with a pattern wheel, treated with 2 μL of 1/eighth water-diluted OS, and incubated during 10 hr into 4 mL sealed glass-vials. The ethylene accumulated in the glass vials was quantified with a photoacoustic spectrophotometer (http://www.sensor-sense.nl) operating at the ET-specific excitation frequency of 1,640 Hz in the sample mode.

2.5 | Quantification of jasmonates, ABA and SA by HPLC coupled to triple quadrupole mass spectrometry

Phytohormones were extracted following the protocol described in Wu, Hettenhausen, Meldau, and Baldwin (2007) with small changes. A total of 200 mg of finely ground tissues were added to 1 mL ethyl acetate spiked with 200 ng of D_2-JA and 40 ng of D_6-ABA, D_4-SA and JA-$^{13}C_6$-Ile as internal standards and metal balls were added. The samples were homogenized in a ball mill (Genogrinder 2000; SPEX CertiPrep) for 45 s at 250 strokes/min. Homogenized samples were centrifuged at 16,000*g*, 4°C for 30 min. Each pellet was re-extracted with 0.5 mL of ethyl acetate and centrifuged. Supernatants were combined and dried in a SpeedVac, and finally resuspended in 0.5 mL of 70% methanol before centrifugation. Phytohormones were detected by high pressure liquid chromatography coupled to a triple quadrupole mass spectrometer as described in Stitz et al. (2011). Chromatography was performed on an Agilent 1200 HPLC system (Agilent Technologies) using a Zorbax Eclipse XDB-C18 column (50 × 3 × 4.6 mm,

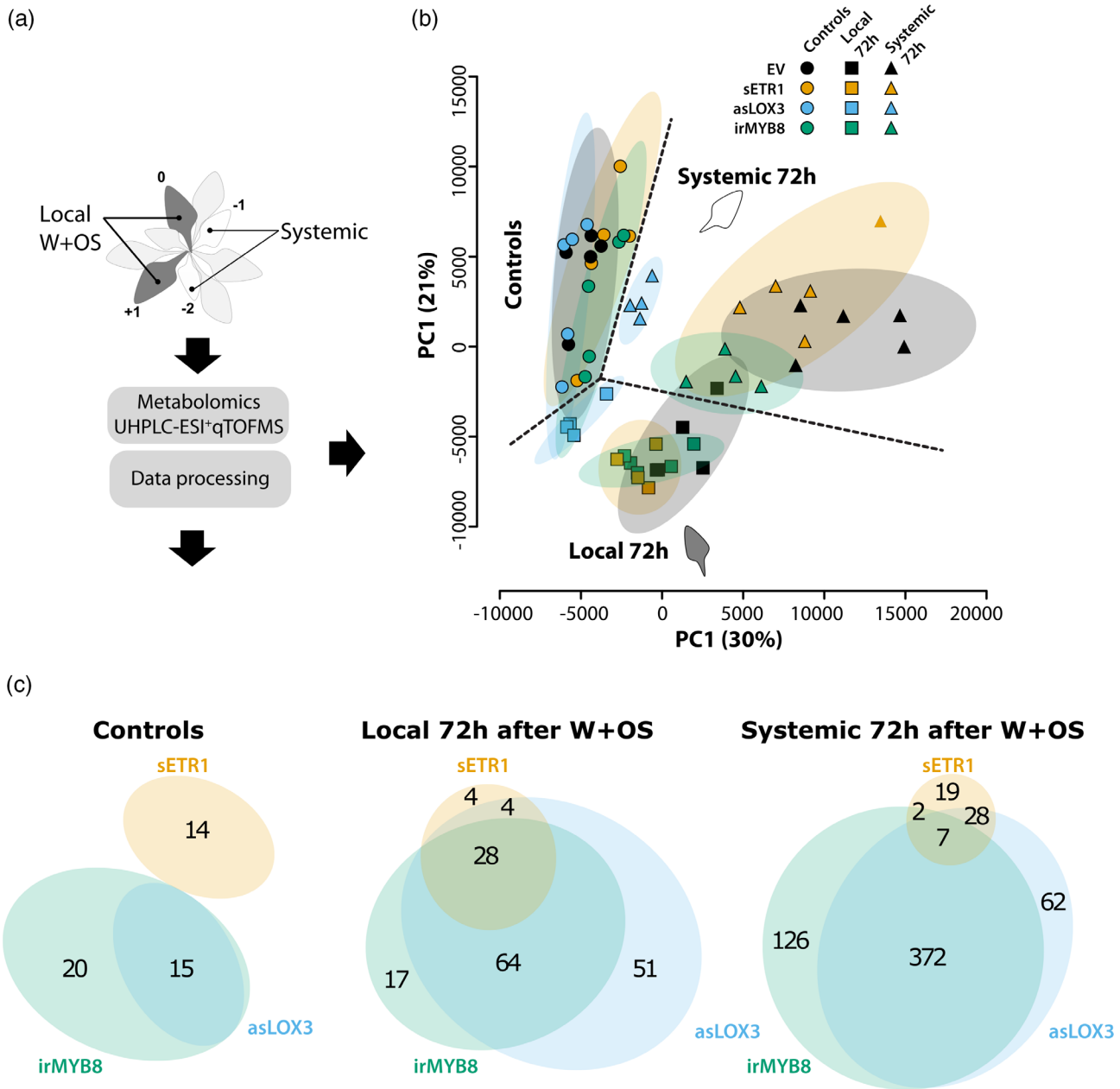

FIGURE 2 Untargeted Mass Spectrometer (MS)-based metabolomics detects distinct herbivory-induced reconfigurations in local and systemic tissues and a major overlap between ethylene-, jasmonic acid- and MYB8-dependent responses in locally elicited leaves. (a) Elicitation scheme and metabolomics workflow to parse local and systemic secondary metabolism to simulated insect herbivory. Two fully expanded rosette leaves were mechanically wounded and treated with diluted oral secretions (W + OS) from *M. sexta*. Untreated systemic leaves growing, with minimal angular distance, above elicited leaves were also collected in the four different genotypes [empty vector (EV), asLOX3, sETR1 and irMYB8] at specific time points after simulated herbivory. Leaf methanolic extracts were subjected to UHPLC-qTOF-MS analysis. MS data were post-processed XCMS and CAMERA R packages to generate a consistent *m/z* feature matrix analysed by univariate and multivariate statistics. (b) Score plot generated for the two first principal components (PCs) derived from a principal component analysis using an autoscaled matrix for *m/z* feature peak intensities extracted for measurements of control (time point 0) and local/systemic W + OS elicitation (72 hr) samples. Dashed ellipses represent 95% Hostelling confidence intervals. (c) Venn diagram visualization of overlapping and non-overlapping significantly deregulated *m/z* features (sampling/tissue-type-specific one-way ANOVA followed by Tukey HSD post hoc tests, $p \leq .01$) in sample measurements of control, local and systemic leaves of each of the transgenic line compared to in the corresponding EVs. Ellipses' size and overlapping areas are respectively proportional to the total number of transgenic line-level deregulated *m/z* features and numbers of overlapping *m/z* features between transgenic lines [Colour figure can be viewed at wileyonlinelibrary.com]

1.8 μm; Agilent). Formic acid (0.05%) in water and acetonitrile were employed as mobile phases A and B, respectively. The elution gradient was based on a binary solvent [time/concentration (min/%) for B]: 0 min/5%, 0.5 min/5%, 9.5 min/42%, 9.51 min/100%, 12 min/100% and 15 min/5%. The solvent A consisted in deionized water with 0.05% formic acid. The solvent B consisted in acetonitrile. The flow rate was constant at 1.1 mL/min and the column temperature was set at 25°C. An API 3200 tandem mass spectrometer (Applied

Biosystems) equipped with a Turbospray ion source was operated in the negative ionization mode. Parent-to-product ion transitions specific to each hormone were monitored: *m/z* 136.9 to 93.0 for SA, *m/z* 140.9 to 97.0 for D_4-SA, *m/z* 209.1 to 59.0 for JA, *m/z* 213.1 to 56.0 for D_2-JA, *m/z* 263.0 to 153.2 for ABA, *m/z* 269.0 to 159.2 for D_6-ABA, *m/z* 322.2 to 130.1 for JA-Ile and OH-JA-Ile, *m/z* 328.2 to 136.1 for JA-$^{13}C_6$-Ile. Quantification was achieved by integrating peak areas of natural phytohormones and comparing them to those of their respective internal standards.

2.6 | Polyamines and tyramine quantification by HPLC-FLD

Free polyamines of ground leaf tissues were quantified using a method described in Docimo et al. (2012). Approximately 50 mg of ground tissues were extracted with 0.1 N HCl and metal balls were added. The samples were homogenized in the ball mill (Genogrinder 2000; SPEX CertiPrep) for 45 s at 250 strokes/min. Homogenized samples were centrifuged at 16,000*g*, 4°C for 30 min. Supernatants were re-centrifuged as before. A supernatant aliquot was added to a borate buffer solution (pH 11). A total of 50 μL of this mix was first derived with 50 μL of OPA (*ortho*-phthalaldehyde) for 1 min, and then a second derivatization with FMOC (fluorenylmethyloxycarbonyl chloride) was applied for 2 min. Polyamines were detected by the fluorescence of OPA molecules bound to primary amines (excitation = 340 nm, emission = 445 nm). The elution gradient was based on a binary solvent [time/concentration (min/%) for B]: 10 min/100%, 13 min/100%, 13.1 min/50% and 14.6 min/50%. Solvent A was deionized water with 0.05% formic acid. Solvent B was pure acetonitrile. The flow rate was constant at 0.8 mL/min and the column temperature was set at 25°C. Quantification of putrescine, spermidine and tyramine was achieved using external calibration curves built from the measurement of authentic standards.

2.7 | Phenolamide quantification by HPLC-PDA

Phenolamides extracted from ground leaf tissues were quantified with a HPLC-photodiode array (PDA) detector as previously described in Onkokesung et al. (2011). Approximately 100 mg of frozen leaf tissue powder was extracted with 1 mL of acidified (0.5% acetic acid) 40% methanol. Small metal balls were added to the samples and those were then homogenized with a ball mill (Genogrinder 2000; SPEX CertiPrep) for 45 s at 250 strokes/min. Homogenized samples were centrifuged at 16,000 g, 4°C for 30 min. A total of 400 μL of each supernatant were transferred to 2-mL glass vials for analysis on an Agilent HPLC 1100 series device (http://www.chem.agilent.com). A total of 1 μL of each sample was injected into a Chromolith FastGradient RP 18-e column (50 × 3 × 2 mm; monolithic silica with bimodal pore structure, macropores with 1.6 mm diameter; Merck) protected by a precolumn (Gemini NX RP18, 2 × 3 × 4.6 mm, 3 mm). The elution gradient was based on a binary solvent system. Solvent A consisted in 0.1% formic acid and 0.1% ammonium water, pH 3.5. Solvent B was pure methanol. The following conditions were applied for the gradient [time/concentration (min/%) for B]: 0.0 min/0%, 0.5 min/0%, 6.5 min/80%, 9.5 min/80% and reconditioning for 5 min to 0% B. The flow rate was constant at 0.8 mL/min and the column temperature was set to 40°C. Phenolamides were detected by operating the PDA at a wavelength of 320 nm. Quantification was performed by building external calibration curves for authentic standards of caffeoylputrescine and chlorogenic acid (CGA). *N′*,*N″*-dicaffeoylspermidine (DCS) isomeric peaks were pooled and reported as total DCS. Since no standard for DCS was available, its content was expressed as CGA equivalents.

2.8 | Untargeted UHPLC-TOF-MS measurements

To achieve a comprehensive view on the secondary metabolite profile of the leaves of the different plant genotypes, an untargeted approach was undertaken by running extracted leaf samples on an Ultra High Pressure Liquid Chromatography (UHPLC) coupled with a Time-of-Flight (TOF) Mass Spectrometer (MS) as described in Onkokesung et al. (2011). Two microliters of leaf extracts, prepared as above, were separated using a Dionex Rapid Separation LC system equipped with a Dionex Acclaim 2.2-mm 120A, 2.1 × 150 mm column. The elution gradient was based on a binary solvent. Solvent A consisted in deionized water with 0.1% acetonitrile and 0.05% formic acid. Solvent B consisted in acetonitrile with 0.05% formic acid. The following conditions were applied for the gradient: 0–5 min, isocratic 95% A, 5% B; 5–20 min, linear gradient to 32% B; 20–22 min, linear gradient to 80% B; isocratic for 6 min. The flow rate was constant at 0.300 mL/min. Eluted compounds were detected by a MicroToF mass spectrometer (Bruker Daltonics) equipped with an ESI source operated in positive ionization mode. Typical instrument settings were as follows: capillary voltage, 4,500 V; capillary exit, 130 V; dry gas temperature, 200°C; dry gas flow of 8 L/min. Ions were detected from *m/z* 200 to 1,400 at a repetition rate of 1 Hz. Mass calibration was performed using sodium formate clusters (10 mM solution of NaOH in 50%:50% isopropanol:water containing 0.2% formic acid).

Raw chromatograms were exported to netCDF format using the export function of the Data Analysis version 4.0 software (Bruker Daltonics) and processed using the XCMS package in R (Smith, Want, O'Maille, Abagyan, & Siuzdak, 2006). Peak detection was performed using the centwave algorithm with the following parameter settings: ppm = 20, snthresh = 10, peakwidth = c(5,18). Retention time correction was accomplished using the XCMS retcor function with the following parameter settings: mzwid = 0.01, minfrac = 0.5, bw = 3. Areas of missing features were estimated using the fillPeaks method. Annotation of compound spectra derived from in-source fragmentation during ionization and corresponding ion species was performed with the BioConductor package CAMERA (Kuhl, Tautenhahn, Böttcher, Larson, & Neumann, 2012). Compound spectra were built with CAMERA according to the retention time similarity, the presence of detected isotopic patterns and the strength of the correlation values

among extracted ion currents of coeluting *m/z* features. CAMERA grouping and correlation methods were used with default parameters. Clustered features were annotated based on the match (±5 ppm) of calculated *m/z* differences versus an ion species and neutral loss transitions rule set. The R script used for XCMS and CAMERA post-processing of the data is provided as Supplemental File S1.

2.9 | Statistical analysis

For the targeted quantitative analysis of polyamine, phenolamide, phytohormone and transcript levels, results were analysed by univariate statistics using native functions in the R environment. Relevant statistical tests applied to the above data-sets are mentioned in figures captions. If normality assumption, or homoscedasticity, was not met, non-parametrical tests, $\log_2$ transformation respectively, were applied. Corresponding statistical results are provided in Supplemental File S4.

In the case of MS metabolomics data, a combination of univariate and multivariate statistical approaches was used for data exploration. The complete 75th percentile-normalized XCMS/CAMERA matrix used as input for the below statistical analyses is available as Supplemental File S2. To diminish redundancy within the data matrix, multi-charged *m/z* features detected by the CAMERA analysis were excluded. *m/z* features consistently detected in at least 75% of the biological replicates of one factorial group were considered for further analysis. Zero values, which remained after application of the 'filling in' function in XCMS, were replaced by one-half of the minimum positive value of the ion across all time points and conditions in the original data. Raw intensity values were 75th percentile normalized before statistical analysis. Metabolite fragmentation patterns were annotated as described in Supplemental File S1. To analyse data structure, PCA analysis was performed using the prcomp package for R via the MetaboAnalyst interface (http://www.metaboanalyst.ca). During this analysis, the data matrix was first scaled using the Pareto scaling procedure and 40% of the *m/z* signals detected as constant based on the examination of their interquantile range, were removed as these variables are unlikely to be used in modelling main trends in the data. In addition, univariate statistical analyses statistical were performed from the metabolomics data matrix to identify genotype-specific and W + OS-specific effects on individual *m/z* features. Briefly, one-way ANOVAs followed by Tukey's Honestly Significant Difference (Tukey's HSD) post hoc tests were carried out on a single time point basis, after $\log_2$-transformation of the original data. The results are visualized as part of the Venn diagrams of Figures 2c and S2 summarizing overlapping and non-overlapping deregulated *m/z* features in each of the tested genotypes. Corresponding statistical results are reported in Supplemental File S3. Heat-maps in Figure 3 summarized statistical effects and fold-change regulation for individual *m/z* features as analysed using *t* tests. In Figure 3, colour-coded $\log_2$-transformed fold changes correspond to those derived from a genotype comparison for which a statistically significant effect ($p < .05$) was detected. In addition to pairwise counter-genotype statistical comparison, W + OS-inducibility of single *m/z* features in the EV background was also analysed by statistically comparing peak areas in the W + OS treated EVs compared to their corresponding untreated controls. Finally, a non-parametric Wilcoxon rank test was used for pairwise comparison between each of the transgenic lines and the EV of the distribution of $\log_2$-transformed fold changes (W + OS vs. untreated controls) obtained for features within the *m/z* cluster 1. Corresponding statistical results are reported in Supplemental File S5.

3 | RESULTS

3.1 | Effect of genetic manipulations of ethylene and jasmonate signalling on simulated leaf herbivory in *N. attenuata*

In the current study, we made use of previously generated transgenic lines that are specifically manipulated in the perception of ET (sETR1), the biosynthesis of jasmonates (asLOX3) and in the expression of MYB8 (irMYB8), a pivotal jasmonate-dependent transcription factor regulating herbivory-induced phenolic metabolism (Figure 1a). Prior to the exploration of metabolomics dynamics in the different transgenic lines, we extended the previous analyses of jasmonate bursts in the sETR1 line. In agreement with previous studies by Onkokesung, Galis, et al. (2010) and von Dahl et al. (2007) on the ET perception-mediated feedback inhibition of ET biosynthesis in sETR1, leaves of the sETR1 line used in the current study emitted twice as much ET over a 10 hr period than those of the EV (Figure 1b). Total ET emissions by asLOX3 and irMYB8 were unaltered compared to that in EV (Figure 1b). Peaking levels of JA were identical in locally elicited leaves of sETR1 plants to those of EV, although a 28% reduction in the levels of JA-Ile was detected (Figure 1c,d). No significant changes were detected for peaking levels of hydroxylated JA-Ile in leaves of sETR1 plants compared to those of EV (Figure 1e). Jasmonate levels had not been previously characterized by Kaur et al. (2010) as part of their phenotyping study on irMYB8 transgenic plants. Here, while locally induced peaking JA levels at 1 hr in leaves of irMYB8 were on average greater than those of EV, no statistically significant differences were detected when comparing jasmonate dynamics in this line and the EV background. Salicylic acid (SA) and abscisic acid (ABA) were also measured in the context of these analyses. Levels of both hormones increased after the W + OS (Figure S1), but no alterations specific to the manipulation of ET signalling were detected.

3.2 | Transgenic lines exhibit overlapping and non-overlapping deregulations of herbivory-induced metabolic responses

To explore the control exerted by phytohormonal cross-talk over herbivory-induced metabolic adjustments, local and systemic leaves of the transgenic lines were collected 0, 24, 48 and 72 hr following simulation of insect herbivory. They were analysed by untargeted MS-

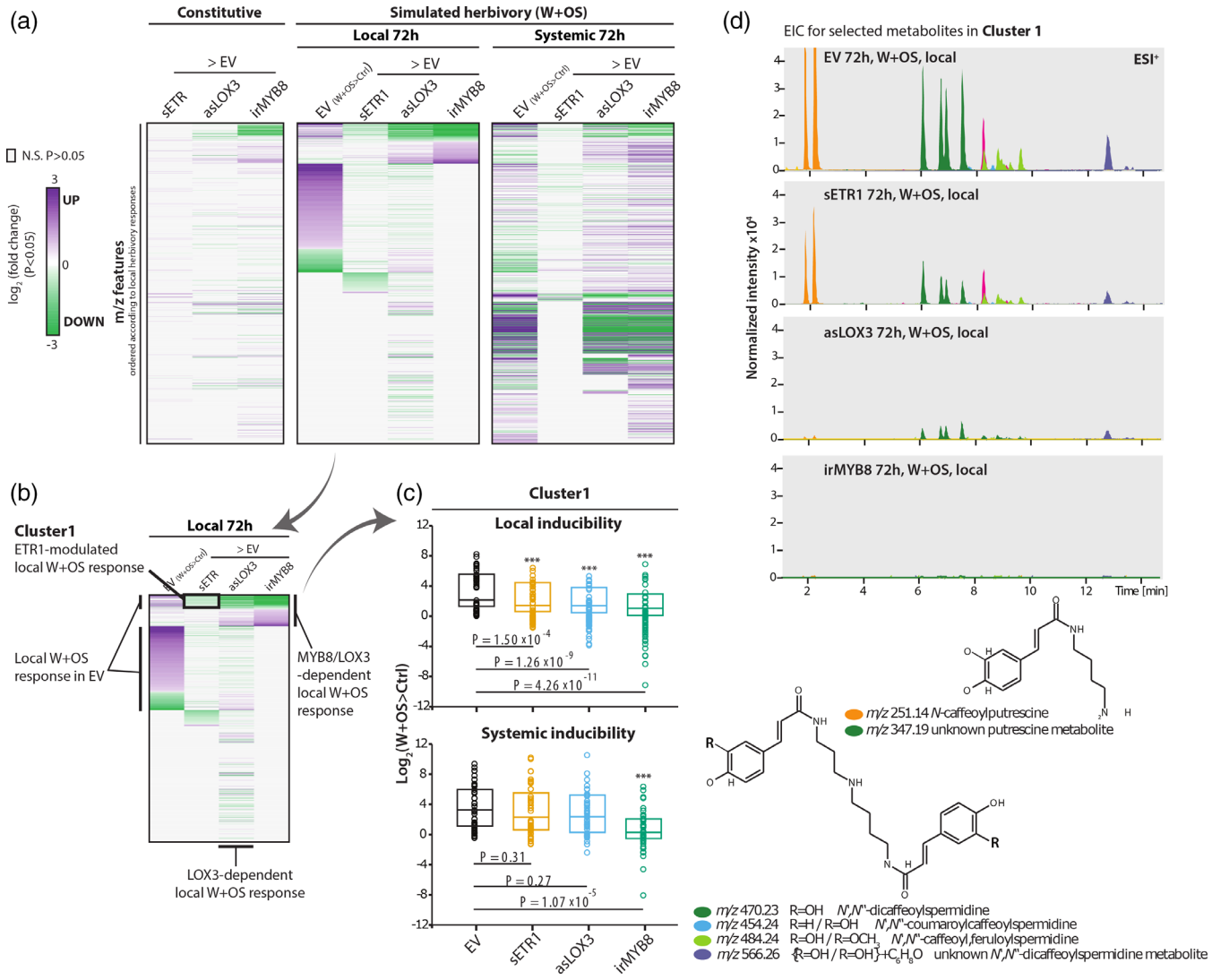

FIGURE 3 Statistical processing of Mass Spectrometer (MS)-based metabolomics data pinpoints on a cluster of JA/MYB8-dependent phenolamides whose local W + OS induction is attenuated in sETR1. (a) Transgenic line-specific deregulations in metabolite signals (*m/z* features): colour-coded cells (green to violet) in the heat-maps denote, unlike grey cells, features for which a statistically significant effect was detected for a given comparison. The first heat-map visualizes constitutive (untreated leaves) deregulation in the three reported transgenic lines compared to in the corresponding empty vector plants (EV). The next two heat-maps focus on local and systemic deregulations at 72 hr after W + OS (simulated herbivory) in sETR1, asLOX3 and irMYB8 compared to the same conditions for the EV. For these two heat-maps the first column depicts *m/z* feature herbivory-regulation in the EV by comparing the level of intensities after W + OS of the concerned features compared to in controls. For both heat-maps, features were sorted according to fold-change regulation in locally W + OS-treated EV to facilitate the exploration of genotype- and tissue-specific regulation of clusters of W + OS-regulated features. All pairwise comparisons involved *t* tests ($p = .05$ as threshold for statistical significance). (b) Annotation of patterns visualized in the 'local' heat-map after ordering of $\log_2$-transformed fold change values according to in the EV, next for the irMYB8 and finally for the sETR1 background. Cluster 1 comprises many *m/z* features induced locally in the EV but whose local induction is strongly impaired in irMYB8/asLOX3 and attenuated in sETR1. (c) Comparison of $\log_2$-transformed fold changes after W + OS only for features of cluster 1. Distributions were statistically compared to in EV by Wilcoxon rank sum tests. (d) Uniformly scaled representative extracted ion currents (electrospray positive, ESI^+) in the different genotypes for *m/z* values corresponding to precursors ($[M + H]^+$ adducts) of phenolamides enriched in cluster 1. Putrescine- and spermidine-based phenolamide annotations are provided [Colour figure can be viewed at wileyonlinelibrary.com]

based metabolomics using an optimized UHPLC-ESI^+-qTOF-MS method that we previously optimized to profile polar-to-semi-polar *N. attenuata* leaf metabolites (Gaquerel, Heiling, Schoettner, Zurek, & Baldwin, 2010). The overall procedure makes use of the power of non-targeted MS metabolomics coupled with statistical analyses to infer overlapping and non-overlapping sets of differentially regulated metabolites across transgenic manipulations of hormonal signalling pathways. A concatenated peak (defined as a mass-to-charge ratio feature, *m/z*, at a single retention time) matrix was exported from the UHPLC-ESI^+-qTOF-MS factorial data-set. This matrix was then subjected to a principal component analysis (PCA). As expected, the resulting PCA score plot showed a clear demarcation between local

and systemic leaf-derived metabolic profiles, as well as between metabolic profiles corresponding to leaves before and after simulated herbivory (Figure 2b). In line with the central role of JA signalling in the activation of herbivory-induced metabolic changes, separation was not as strong in asLOX3 plants as in the other genotypes. *m/z* features exhibiting greatest loading values for sample clustering according to the two principal components (PC; Figure 2b) corresponded to nicotine ($[M + H]^+$: $C_{10}H_{15}N_2^+$, *m/z*: 163.12, loading PC1: 0.44) and several phenolamides, such as CP ($[M + H]^+$: $C_{13}H_{19}N_2O_3^+$, *m/z*: 251.14, loading PC1: 0.33) and DCS ($[M + H]^+$: $C_{25}H_{32}N_3O_6^+$, *m/z*: 470.23, loading PC2: 0.15). To compare metabolic responses in the different transgenic lines, the overlap of significantly deregulated *m/z* features in asLOX3, irMYB8 and sETR1 plants (compared to in EV) was investigated by means of Venn diagrams (Figures 2c and S2). The latter analysis revealed that the identity of deregulated *m/z* features in asLOX3 and irMYB8 plants largely overlapped in the two leaf positions collected, while deregulated features in sETR1 plants only partly overlapped for locally elicited leaves with those inferred in asLOX3 and irMYB8 genetic backgrounds.

3.3 | ET-insensitivity differentially alters local and systemic metabolic responses to simulated herbivory

To further parse the most important metabolic deregulations activated in each of the different transgenic lines, we conducted univariate statistical analyses using the *m/z* feature concatenated matrix and visualized statistical results as heat-maps (Figure 3). Briefly, the first heat-map of Figure 3 visualizes constitutive (untreated leaves) deregulation in the three transgenic lines compared to the corresponding empty vector plants (EV). The next two heat-maps focus on local and systemic deregulations at 72 hr after W + OS treatment in sETR1, asLOX3 and irMYB8 compared to the same conditions for EV. We further ranked *m/z* features according to most important statistical changes in locally induced EV to identify clusters of W + OS-regulated features and visualize how the corresponding core-set of metabolites was regulated in the different transgenic lines. This data exploration approach confirmed that, as expected, the majority of locally induced *m/z* features in EV was significantly down-regulated in asLOX3 plants. Those down-regulations were even more pronounced in systemically induced leaves. Similarly, the impact of silencing MYB8, as seen in the down-regulation of many herbivory-induced *m/z* features, was most clearly apparent in systemically induced leaves. From the examination of heat-maps for local metabolic responses, one cluster, referred to as 'cluster 1', was particularly noteworthy. This cluster comprises herbivory-induced *m/z* features severely down-regulated in asLOX3 and irMYB8 and with less pronounced statistical effect of down-regulation in sETR1. Overall, the inducibility of cluster 1 was significantly reduced in locally induced leaves of the three transgenic lines, while a statistically significant reduction of cluster inducibility was only detected for the irMYB8 line when considering systemic leaf metabolic profiles (Figure 3b,c). Extracted ion chromatograms for some of the most abundant *m/z* features in cluster 1, which corresponded to protonated adducts of previously characterized MYB8-dependent phenolamides, confirmed down-regulations in the accumulations of these compounds in leaves of sETR1 plants locally elicited by the W + OS treatment.

Table 1 summarizes fold-change deregulations in the intensity of *m/z* signals characteristics for those and other phenolamides previously structurally identified or annotated based on diagnostic fragments (Gaquerel et al., 2010; Onkokesung et al., 2011). As indicated in previous studies (Onkokesung et al., 2011), the complete detectable phenolamide chemotype was abolished in irMYB8 plants, while deficiency in JA signalling (asLOX3) led to a weaker suppression of these phenolic derivatives. In asLOX3 systemic leaves, several di-acylated spermidine isomers were up-regulated compared to in EV, suggesting that jasmonate-signalling may also more subtly contribute in balancing the production of the different spermidine-containing phenolamides. Within cluster 1, *N*-caffeoylputrescine, which was previously detected as one of the most strongly induced phenolamides in *N. attenuata* upon insect herbivory (Kaur et al., 2010; Onkokesung et al., 2011), appeared as the one most significantly affected by the insensitivity to ET (Table 1 and Figures 4 and 5). Consistent with a tuning effect of ET over the phenolamide chemotype rather than a complete pathway-level control, subtle remodelling of phenolamide levels was detected in locally elicited sETR1 leaves. In particular, only a sub-part of the profile of spermidine-based phenolamides (*N′*,*N″*-dicaffeoylspermidine and *N′*,*N″*-caffeoyl,feruloyspermidine) exhibited a significant reduction in herbivory-induction in sETR1 plants, albeit not to the extent of the dramatic down-regulation effects as seen in irMYB8 and asLOX3 (Figure 4).

We additionally conducted a smaller-scale metabolomics profiling of a previously characterized irACO transgenic line which is silenced for the ACC OXIDASE and hence biosynthetically repressed for ET production (-Figure S3). In contrast with the sETR1 line, which did not exhibit major vegetative growth defects, the irACO line, under our experimental conditions, exhibited a delay in rosette growth compared with EV and stress symptoms (notably numerous necrotic spots detected onto leaves), which hampered its initial use in the larger metabolomics exploratory approach. Similarly to sETR1, locally induced levels of several phenolamides were reduced in irACO compared with EV (Figure S3).

Previously, we reported that the metabolic tension in coumarate allocation between polyamine- and quinate-hydroxycinnamate conjugates is exacerbated during herbivory (Gaquerel, Kotkar, Onkokesung, Galis, & Baldwin, 2013). In the present study, free coumarate and its derivative *O*-coumaroylquinate over-accumulated in local and systemic leaves of irMYB8 plants during simulated herbivory (Figure S4). The latter result indicates that irMYB8 plants, which barely produced phenolamides, likely channelled coumarate units not conjugated to polyamines towards the production of quinate derivatives.

3.4 | ET perception is required for intact local herbivory-induced levels of the two most abundant phenolamides

Next, we conducted targeted quantitative analyses for the two most abundant phenolamides, namely CP and DCS. Their relative levels

TABLE 1 Known metabolites measured by UHPLC-TOF-MS in local leaves after simulated herbivory, which are differentially regulated by the jamonate, ethylene and MYB8 pathways

Compound	Precursor *m/z*	Retention time	Fold change in local leaves 72 hr after simulated herbivory (Unpaired *t* test)			
			W + OS inducibility (W + OS EV 72 hr > EV 0 hr)	JA regulation (W + OS asLOX3 72 hr > W + OS EV 72 hr)	ET regulation (W + OS sETR1 72 hr > W + OS EV 72 hr)	MYB8 regulation (W + OS irMYB8 72 hr > W + OS EV 72 hr)
N-Coumaroylputrescine ($C_{13}H_{19}N_2O_2^+$)	235.14	161 s	**278.2***	**N.D.**	0.7	**N.D.**
		201 s	**41.5****	**N.D.**	0.5	**N.D.**
N-Caffeoylputrescine ($C_{13}H_{19}N_2O_3^+$)	251.14	114 s	**38.5*****	**N.D.**	**0.5****	**N.D.**
		132 s	**13.5*****	**N.D.**	**0.4***	**N.D.**
N-Feruloylputrescine ($C_{14}H_{21}N_2O_3^+$)	265.15	195 s	**39.9*****	**0.1*****	0.7	**N.D.**
		248 s	**98****	**0.1****	0.7	**N.D.**
Putative acylated putrescine ($C_{19}H_{27}N_2O_4^+$)	347.19	542 s	**300****	**0.1****	0.6	**N.D.**
		627 s	301.4	**N.D.**	0.4	**N.D.**
N′-*N″*-Coumaroylcaffeoylspermidine ($C_{25}H_{32}N_3O_5^+$)	454.23	462 s	**3.2***	**0.1****	0.6	**N.D.**
		537 s	1.2	**N.D.**	**0.4***	**N.D.**
N′-*N″*-Dicaffeoylspermidine ($C_{25}H_{32}N_3O_6^+$)	470.23	365 s	1.3	**0.3***	**0.6***	**N.D.**
		412 s	0.9	**0.4****	**0.5***	**N.D.**
		449 s	0.6	**0.4****	**0.4***	**N.D.**
N′-*N″*-Feruloylcaffeoylspermidine ($C_{26}H_{34}N_3O_6^+$)	484.24	492 s	**2.7****	**0.3****	**0.7***	**0.01*****
		526 s	**1.8***	**0.3*****	**0.5***	**0.01*****
		550 s	1.6	**0.2****	**0.6***	**N.D.**
		573 s	1.1	**0.2****	**0.5****	**N.D.**
N′-*N″*-Diferuloylspermidine ($C_{27}H_{36}N_3O_6^+$)	498.26	623 s	**1.6***	**0.5***	**0.7***	**N.D.**
		664 s	1.3	**0.4***	**0.6***	**N.D.**
		696 s	0.7	**0.2***	0.5	**N.D.**
Unknown *N′*-*N″*-Diacylatedspermidine ($C_{31}H_{40}N_3O_7^+$)	566.28	759 s	0.9	0.5	**0.6***	**N.D.**
		807 s	1.8	**0.4***	**0.4***	**N.D.**
Coumaric acid ($C_9H_9O_3^+$)	147.04	528 s	0.9	1.2	0.6	**4.3***
Phenylalanine ($C_9H_{12}NO_2^+$)	166.09	126 s	0.8	0.8	1.1	**0.7***
Tyrosine ($C_9H_{12}NO_3^+$)	182.08	96 s	**0.6***	**1.4***	0.9	1.1
O-Coumaroylquinate ($C_{16}H_{19}O_8^+$)	339.11	420 s	**0.5***	1.5	**0.4***	**5.7***
		528 s	0.6	1.5	0.5	**7.0***
Attenoside ($C_{44}H_{74}O_{21}NH_4^+$)	956.5	1,338 s	**1.7****	**0.6***	0.9	0.8
Nicotianoside I ($C_{41}H_{66}O_{19}Na^+$)	885.41	1,356 s	0.9	**0.6***	0.7	0.9
Lyciumoside II ($C_{38}H_{64}O_{17}Na^+$)	815.39	1,344 s	0.7	0.9	**1.5***	1.3
Lyciumoside IV (fragment, $C_{26}H_{41}O_4^+$)	471.17	1,338 s	**1.9****	**0.5***	0.8	0.8

Note: Rosette leaves of wild-type, asLOX3, sETR1 and irMYB8 plants were wounded and treated with diluted oral secretion of caterpillars (W + OS treatment). Leaves before and 72 hours after the treatment were harvested, and their metabolites were extracted with acidified methanol. Extracts were subjected to mass spectrometry analysis using UHPLC-qToF-MS. *m/z* features were recorded for different elution times and analysed using Metaboanalyst. According to previous studies, some *m/z* features could have been assigned to known compounds (Gaquerel et al., 2010; Onkokesung et al., 2011). Only known compounds that were differentially regulated in at least one genotype are presented. Fold change were calculated either by comparing treated leaves with control leaves in wild-type (local inducibility) or by comparing treated leaves in the different genotypes with treated leaves in wild-type. Unpaired *t* tests were calculated from metaboanalyst-analysed data and sample weights were taking into account to normalize peak area. Significant up- and down-regulations are highlighted in bold font. These regulations are due to W + OS elicitation (local inducibility) or RNAi silencing (asLOX3, sETR1 or irMYB8).

Abbreviation: N.D., not detected.

*$p < .05$; **$p < .01$; ***$p < .001$.

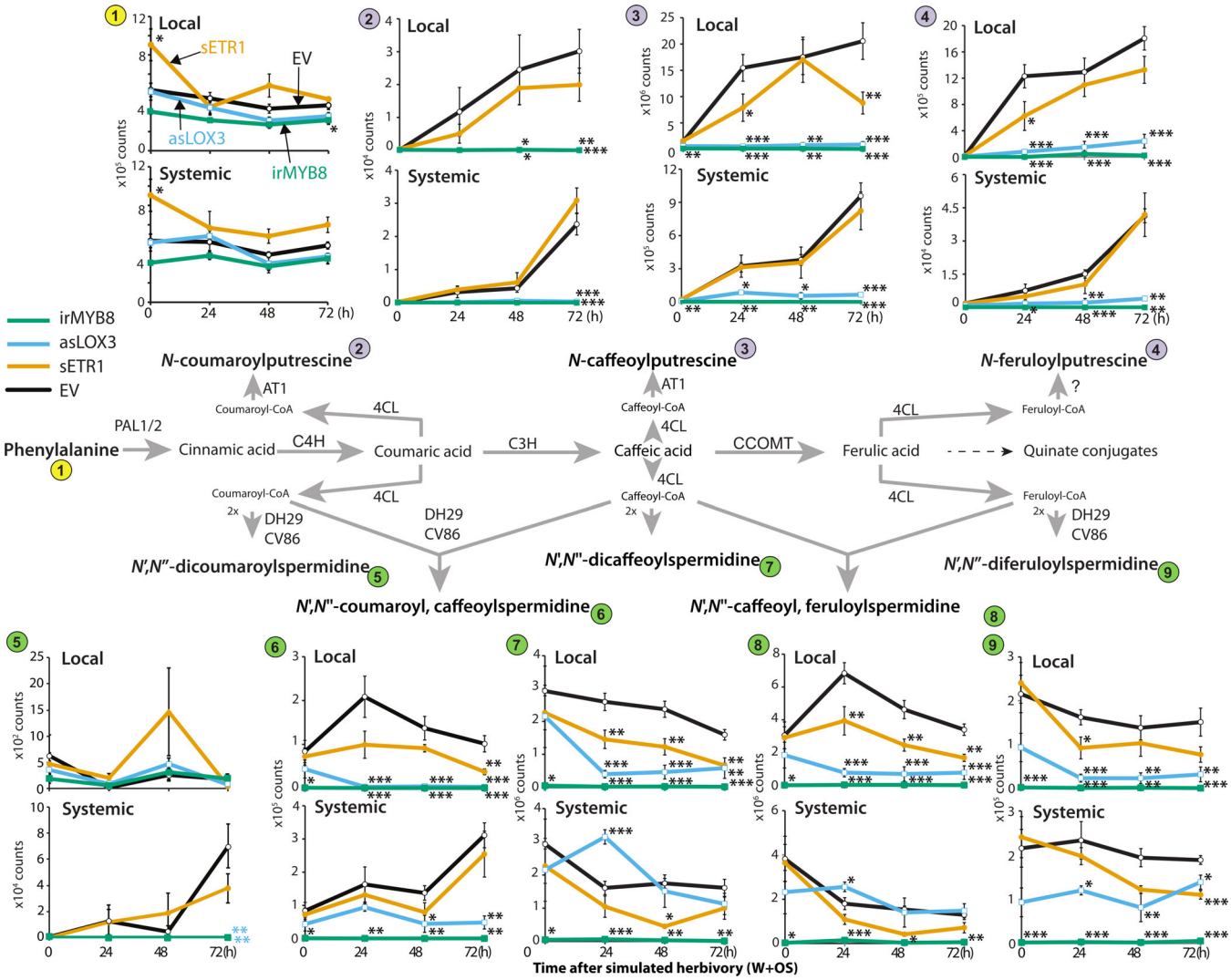

FIGURE 4 Local accumulation dynamics of JA/MYB8-dependent phenolamides in response to W + OS elicitation are modulated by ET in *N. attenuata*. Mean values (±*SE*, four to five biological replicates) of phenolamides and phenylalanine main *m/z* features in local and systemic leaves during simulated herbivory. Asterisks indicate significant differences with EV at respective time points (**p* < .05, ***p* < .01, ****p* < .001, ANOVA followed by Tukey HSD post hoc tests). Leaves from EV, sETR1, asLOX3 and irMYB8 plants were harvested at different time points before and after W + OS treatment (wounding and oral secretions). Their metabolites were extracted with acidified methanol and subjected to mass spectrometry analysis using UHPLC-qToF-MS operating in positive mode. Only *m/z* features of phenylalanine and known phenolamides were kept for further analysis. The biosynthetic pathway of phenolamides from phenylalanine and phenylpropanoids is depicted. Enzymes are indicated above and below reaction arrows [Colour figure can be viewed at wileyonlinelibrary.com]

appeared, in our metabolomics data-set, to be modulated locally by the ET signalling sector (Figure 5). Targeted analyses are instrumental in confirming trends detected in the untargeted metabolomics approach. As we previously reported in the untargeted approach, CP levels dramatically increased in response to W + OS treatment. This effect was stronger in undamaged (systemic) leaves than in local leaves: CP accumulated four times more in systemic leaves at 72 hr. Our quantitative analyses confirmed that CP and DCS were down-regulated in asLOX3 and sETR1 plants compared to EV plants (Figure 5). Levels of these two compounds in sETR1 plants were intermediary to those detected at corresponding sampling times in EV and asLOX3 plants. Impairing ET signalling in the sETR1 line significantly reduced the production of CP and DCS only in local leaves (by 62 and 64% at 72 hr, respectively; Figure 5b), but not in systemic leaves (Figure 5c). Finally, in contrast with previous studies (Kaur et al., 2010; Onkokesung et al., 2011), we did not detect in our analyses an induction of total DCS levels in response to the W + OS treatment (Figure 5b,c). Total DCS levels were nearly constant, or slightly decreased, during the time-course experiment in response to the elicitation.

3.5 | ET signalling does not affect levels of free polyamines during simulated herbivory

We then explored whether local herbivory-induced ET production influences polyamine homeostasis for phenolamide production as a result of the shared SAM precursor (Figure 1a). To this end, we quantified the

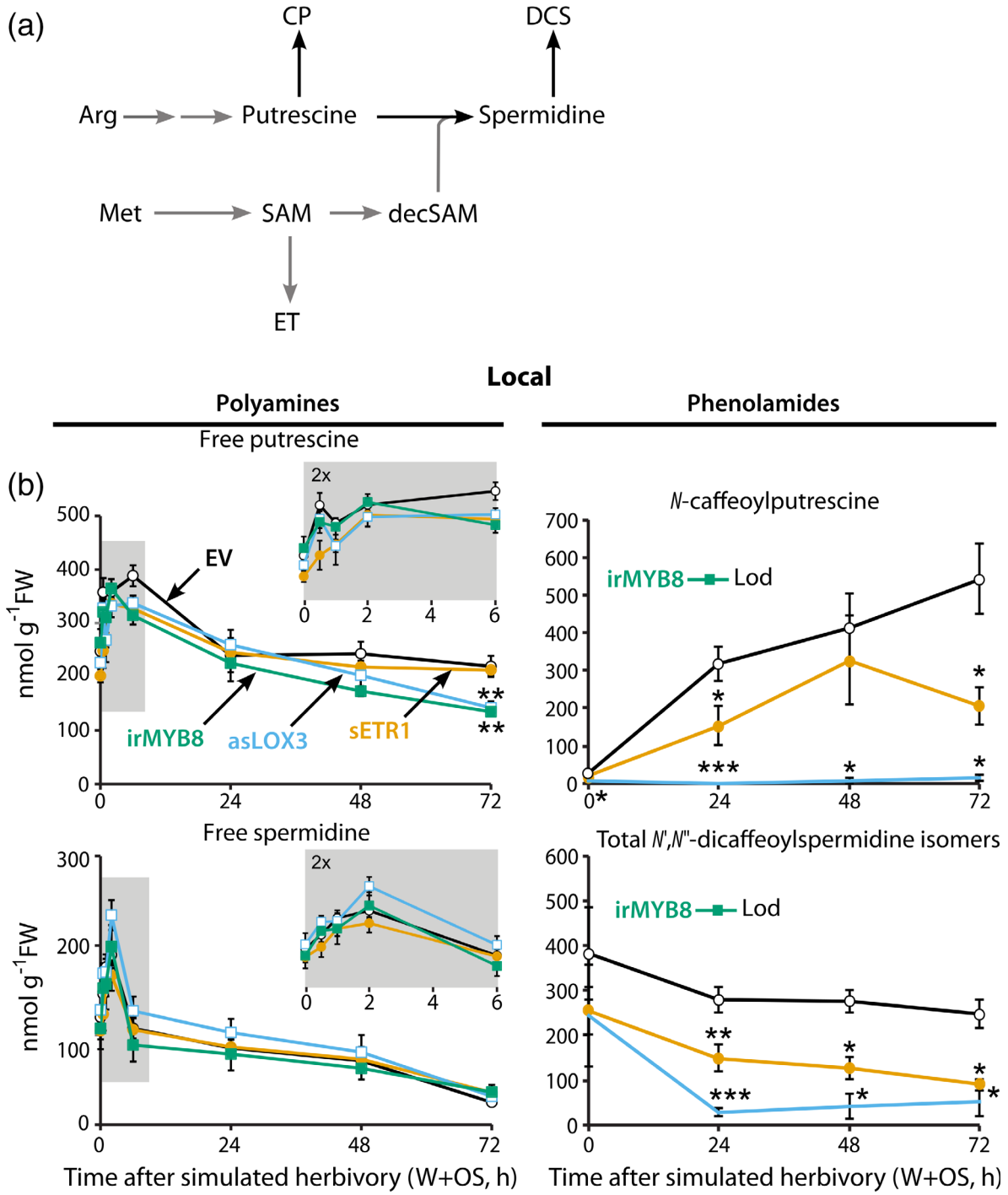

FIGURE 5 Targeted HPLC-UV analysis of free polyamines and phenolamides indicate that the ethylene pathway modulates phenolamide accumulation after herbivory, without any influence on polyamines pathway. (a) Schematic pathway depicting biochemical connections between ethylene and polyamine synthesis and acylation of polyamines into *N. attenuata* main phenolamides (in black). Arg, arginine; CP, caffeoylputrescine; DCS, dicaffeoylspermidine; decSAM, decarboxylated-*S*-adenosylmethionine; ET, ethylene; Met, methionine; SAM, *S*-adenosylmethionine. (b,c) Mean values (±*SE*, five biological replicates) of free polyamines and phenolamides in local and systemic leaves, respectively, after simulated herbivory (wounding and oral secretions, W + OS). Leaves from EV, sETR1, asLOX3 and irMYB8 plants were harvested at different time points before and after W + OS treatment. 'Systemic' refers to undamaged young leaves. Free polyamines levels were measured by HPLC-UV in leaves extracts subjected to derivatization and quantified with appropriate standards. Insets show details on the dynamic induction of free polyamines at early time points of the same experiment. Phenolamides levels were measured from leaves extracts by HPLC-PDA and quantified with appropriate standards when available. DCS are thus reported as CGA equivalent. DCS levels are a pool of the different DCS isomers that were detectable. Phenolamides were undetectable in irMYB8 plants (Lod). ANOVA tests followed by Tukey HSD post hoc tests were applied to free polyamines and phenolamides levels at each time point. When normality assumption was not met, Kruskal–Wallis and pairwise Wilcoxon rank sum tests were applied. Only significant differences between EV plants and sETR1, asLOX3 or irMYB8 plants are reported. *$p < .05$, **$p < .01$, ***$p < .001$ [Colour figure can be viewed at wileyonlinelibrary.com]

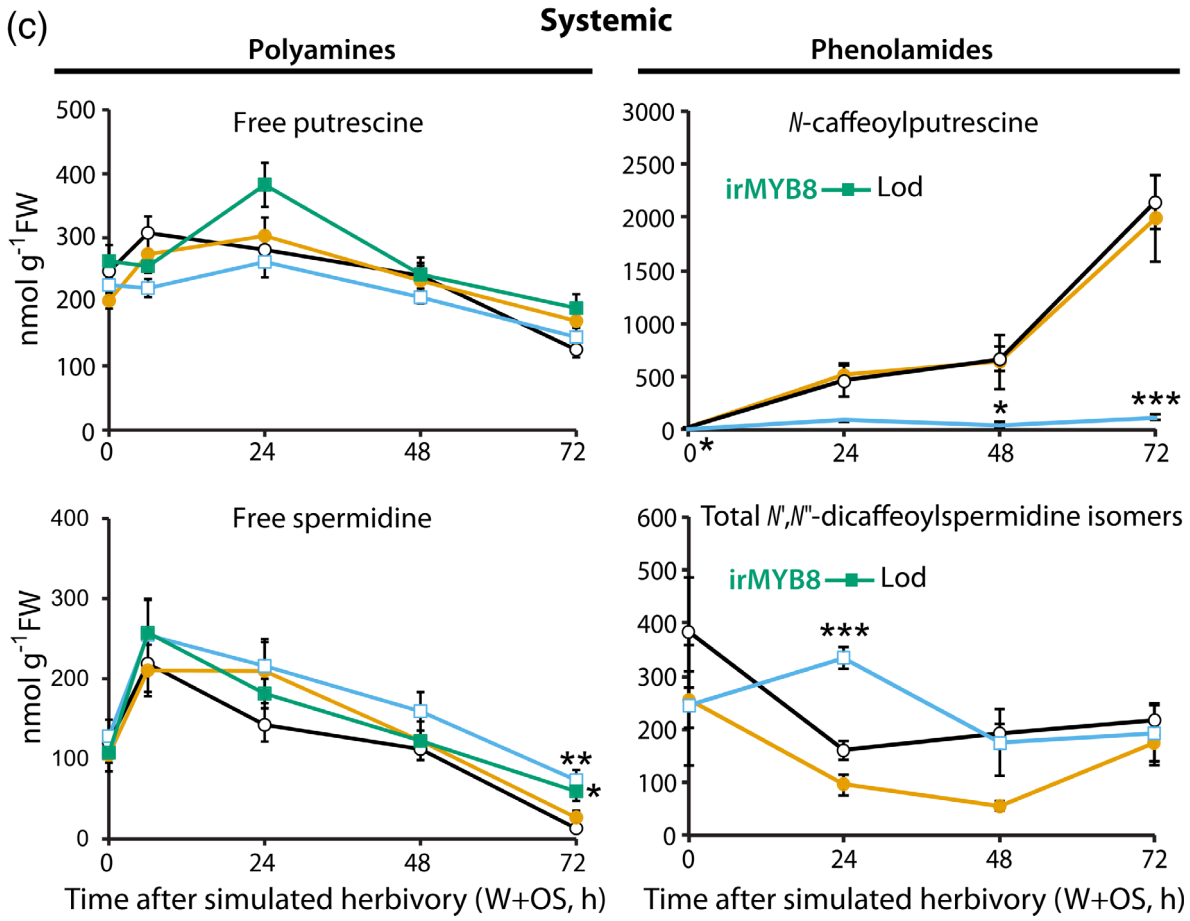

FIGURE 5 (Continued)

time-course changes in levels of free putrescine, spermidine and spermine in leaf tissues after simulated herbivory. The extent to which the pools of theses amines are reconfigured during insect herbivory had remained, to our knowledge, largely unexplored. Constitutive amine levels were not statistically different among transgenic lines and the EV (Figure 5b,c). Upon W + OS treatment, spermidine levels decreased consistently in all lines in both local and systemic tissues, resulting in up to 10 times less free spermidine detected in EV plants at 72 hr compared to prior treatment (Figure 5b). While strongly decreased because of the W + OS treatment, levels of spermidine in systemic leaves of asLOX3 and irMYB8 collected at 72 hr were significantly higher than those in EV. In locally treated leaves, spermidine and putrescine exhibited transient elevations, albeit weaker in the case of putrescine, in response to the simulated herbivory (Figure 5b). Putrescine levels measured at 72 hr in local leaves were significantly reduced by 60% compared to those in EV. Importantly, putrescine and spermidine levels in sETR1 did not differ from those in EV (Figure 5).

3.6 | Free tyramine levels strongly increase in locally elicited leaves

We additionally quantified tyramine, an arylamine that can be acylated with hydroxycinnamic units to form an additional group of herbivory-induced phenolamides, not detected in our metabolomics screen (Bassard, Ullmann, Bernier, & Werck-Reichhart, 2010; Kim, Yon, Gaquerel, Gulati, & Baldwin, 2011). Of all amine analysed in this study, tyramine exhibited the strongest response to the simulated herbivory treatment with locally induced levels, reaching up to 15 times those quantified prior to elicitation of EV plants (Figure S5). In contrast, asLOX3 and MYB8 plants, but not sETR1 plants, accumulated less tyramine in local leaves 72 hr after simulated herbivory (Figure S5). Intrigued by the strong local accumulation of tyramine and its possible direct role as a defence compound per se, we conducted *M. sexta* larval performance assays on artificial diet supplemented with different doses of tyramine. No significant effect of tyramine on *M. sexta* weight gain was detected (Figure S6).

3.7 | Silencing ethylene perception does not significantly alter the transcription of MYB8, PAL2, AT1, DH29 and CV86

Since the effect of ET on the jasmonate-/MYB8-dependent induction of phenolamide production did not appear to result from modulations in the homeostasis of free polyamines, we finally quantified the transcript levels of genes involved in the

biosynthesis of phenolamides. As expected, transcript levels of *MYB8*, *PAL2*, *AT1*, *DH29* and *CV86* strongly increased after simulated herbivory compared with corresponding controls (Figure 6). As previously shown (Gális et al., 2006; Kaur et al., 2010; Onkokesung et al., 2011), expression of the selected genes was compromised in asLOX3 and irMYB8. Only marginally significant reductions in transcript levels of *MYB8* and *CV86* were detected in sETR1 compared to EV (Wilcoxon rank sum tests; p = .095 and .063, respectively).

4 | DISCUSSION

Multiple phytohormone signalling sectors are activated in damaged tissues when plants are attacked by phytophagous insects. However, the mechanistic basis of the interplay between these phytohormones and the breadth of defence traits under its control are not fully understood (Broekgaarden, Caarls, Vos, Pieterse, & Van Wees, 2015; Song, Qi, Wasternack, & Xie, 2014). In the present study, we combined exploratory MS-based metabolomics and analytical approaches

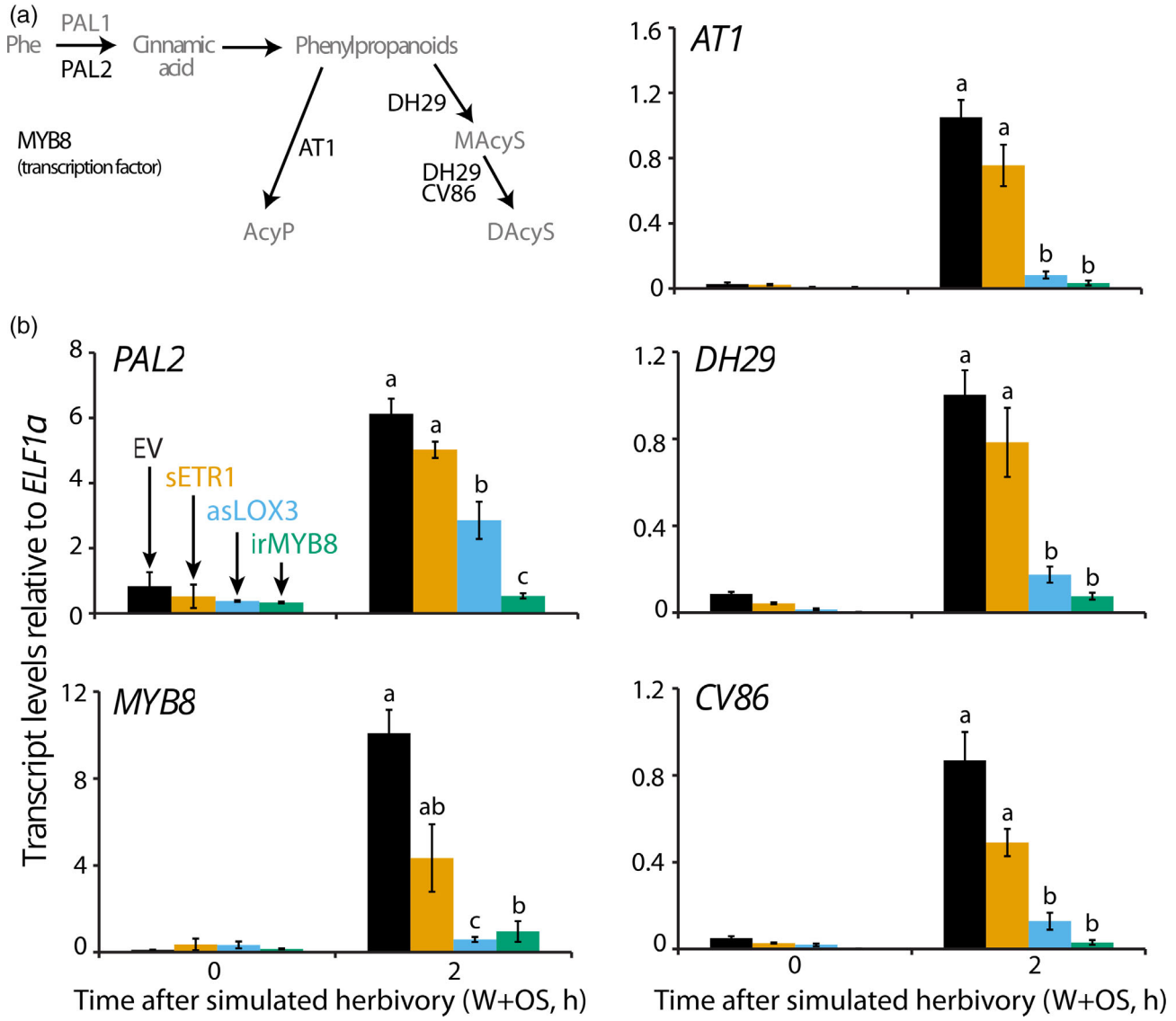

FIGURE 6 Ethylene insensitivity in sETR1 marginally affects the transcription of phenylpropanoid-phenolamide-related genes. (a) Involvement of four enzymes and one transcription factor in phenolamides production: phenylalanine ammonia lyase (PAL), MYB8 (transcription factor), AT1, DH29 and CV86. Enzymes whose gene transcriptions have been measured are in black font. AcyP, acylated putrescine; DAcyS, di-acylated spermidine; MAcyS, mono-acylated spermidine; Phe, phenylalanine. (b) Mean values (±*SE*, four to five biological replicates) of relative transcript of *PAL2*, *MYB8*, *AT1*, *DH29* and *CV86* in control (time point 0) and local leaves 2 hr after simulated herbivory (wounding and oral secretions, W + OS). Different letters indicate statistically significant differences between genotypes (p < .05, one-way ANOVA followed by Tukey HSD post hoc tests; when normality assumption was not met, Kruskal–Wallis and pairwise Wilcoxon rank sum tests were applied) [Colour figure can be viewed at wileyonlinelibrary.com]

targeted to phytohormones, phenolamides, polyamines, as well as relative quantifications of specific transcripts to gain new insights on ET, JA and MYB8 pathways in the response to *M. sexta* attack. Altogether, our results demonstrate that ET acts as an accessory signal for local JA-dependent reconfigurations of the phenolamide chemotype, providing new insights into the coupling between polyamine and phenolamide metabolisms and further highlighting a role for ET in the production of nitrogen-containing defence molecules.

Phenolamides have been characterized as herbivory- and JA signalling-induced metabolites against herbivores in *N. attenuata* (Kaur et al., 2010) and in other Solanaceae (Tebayashi et al., 2007), as well as in rice (Alamgir et al., 2016) and in maize (Marti et al., 2013). Previous work from our group has shown that, while more intense due to repeated elicitation generated by the progress of larval feeding, inductions in phenolamide levels detected during the interaction between *N. attenuata* and *M. sexta* larvae are largely recapitulated by the W + OS elicitation procedure (Kaur et al., 2010; Onkokesung et al., 2011). Virtually any signalling node that influences jasmonate pools is likely to alter induced phenolamide levels. In the present study, the metabolomics data exploration strategy identified intact ET signalling as being necessary to sustain full phenolamide production in locally elicited leaves. The importance of ET in this response, as observed in the sETR1 plants, which are 'deaf' to ET, was further observed in a smaller scale-profiling approach in the irACO line, which is biosynthetically repressed for ET production. Other studies have recently uncovered a role of ET signalling for phenolamide metabolism. For instance, in *Arabidopsis thaliana*, the transcription of phenolamide-related genes was found to be triggered to higher levels of expression when both the JA and the ET pathways were simultaneously activated (Li et al., 2018). In rice, JA and ET signalling are both required for the elevated production of phenolamides in response to the infestation of the white-backed planthopper *Sogatella furcifera* (Wang et al., 2020).

In a recent large-scale metabolomics study, the degree of plasticity and diversity of the specialized metabolic profile of different *Nicotiana* species was investigated in response to herbivory by a 'specialist' (*M. sexta*) and a 'generalist' (*Spodoptera littoralis*, the cotton leaf worm) chewing insects (Li et al., 2020). It was identified that, while JA is the central signal shaping the amplitude of convergent metabolic responses to both herbivories, ET fine-tunes the specificity of this metabolic response according to the herbivore diet breadth. The latter study, as in the present one, detected that phenolamides are the foliar metabolites whose production is most tightly dependent on fine-tuning by ET signalling (Li et al., 2020). This convergence further reinforces a role of ET in mitigating the production of these metabolites according to insect herbivory type and echoes the ecological implications suggested for the well-known function of ET in antagonizing the JA-dependent accumulation of nicotine when tobacco plants are attacked by nicotine-tolerant *M. sexta* larvae. It would be interesting to test whether deregulations in phenolamide levels in sETR1 compared to EV are also attenuated during herbivory by *S. littoralis* or *S. exigua*, whose OS do not elicit ET in *N. attenuata* compared to *M. sexta* (Diezel, von Dahl, Gaquerel, & Baldwin, 2009; Li et al., 2020). Finally, our study confirms that ET oppositely affects JA-regulated nicotine and phenolamide levels.

The fact that deregulations in phenolamide levels in sETR1 were only observed in locally elicited leaves suggests a convergence of JA- and ET-dependent signalling in damaged cells. In this respect, previous work has shown that the interplay of JA and ET signalling at sites of mechanical damage during a W + OS treatment in *N. attenuata* mitigates cell division and tissue regrowth (Onkokesung, Galis, et al., 2010), but the regulatory bases to this response has remained elusive. Other phytohormonal cross-talks are known to affect induced phenolamide levels such as that between the JA and cytokinin pathways (Schäfer, Meza-Canales, Brütting, Baldwin, & Meldau, 2015). The ET pathway could act on several levels for the JA-dependent production of phenolamides. A possible layer of signalling regulation would be associated with an effect of herbivory-elicited ET on jasmonate levels. However, it is very unlikely that the moderate decrease of JA-Ile levels detected in this study could solely account for the pattern of phenolamide accumulation in sETR1 plants. In addition, deregulations in OS-elicited metabolic profiles extracted from sETR1 and asLOX3 locally elicited leaves relatively poorly overlapped. In contrast, the strong overlap between MYB8- and JA-dependent metabolic regulation is consistent with the idea that MYB8 transcription factor activity more broadly influences defence regulation than only phenolamide accumulation (Schäfer et al., 2017).

The biochemical basis of the effect of ET on phenolamide levels was also examined. Indeed, a large body of literature on the parallel occurrence of ET and polyamine biosynthesis in certain tissues has long questioned whether SAM utilized for both metabolisms is rate limiting for either pathway (Bassard et al., 2010; Wuddineh, Minocha, & Minocha, 2018). This hypothesis of a metabolic tension between these two pathways has been tested in the context of several developmental responses including seedling development and fruit ripening. For the latter development context, flux experiments on tomato fruits concluded that ET and polyamines can be synthesized simultaneously without exacerbating the competition for SAM (Lasanajak et al., 2014). Such flux studies have been more rarely undertaken in the context of plant responses to biotic stresses. Transgenic tomato lines overexpressing a yeast spermidine synthase involved in polyamine biosynthesis resulting in a down-regulation of ET biosynthesis and signalling were found to be more susceptible to infection by *Botrytis cinerea* than were WT plants (Nambeesan et al., 2012). Such deregulation of ET signalling and an increase in susceptibility to the biotic stress was not observed when these tomato lines were challenged by *M. sexta* herbivory (Nambeesan et al., 2012). These results suggest that genetically engineering a strong increase in the polyamine biosynthetic flux does not alter the likely key signalling function of the ET signalling sector for defence induction against *M. sexta* in tomato.

In the present study, levels of free polyamines in leaf tissues prior and in the first 72 hr after simulated herbivory did not differ between EV and sETR1 plants, though the amplitude of the ET burst had doubled in sETR1 plants. Our data further indicate that the turnover of polyamines likely exceeds the production rate of the two key phenolamides measured, CP and DCS. Thus, the greater production of ET in sETR1 plants may not be sufficient to deplete the pool of SAM engaged by polyamine biosynthesis. These results are hence in line

with the above-mentioned study which did not detect alterations in ^{14}C incorporation from SAM to ET in transgenic lines producing high levels of spermidine during tomato fruit ripening (Lasanajak et al., 2014). Finally, free putrescine levels, whose production does not depend on SAM, did not accumulate in our study to higher levels in local leaves after simulated herbivory, as would normally be expected if less putrescine molecules were converted into spermidines from a diversion of SAM for ET synthesis.

Tyramine exhibited, from all analysed amines, the most pronounced response to the simulated herbivory treatment. While earlier metabolomics studies conjointly detected herbivory-induced tyramine-containing phenolamides in leaves in sand-grown *N. attenuata* (Kim et al., 2011), the present and a recent metabolomics analyses (Gaquerel et al., 2010; Li et al., 2020) did not detect the presence of such metabolites in herbivory-induced profiles. It is unclear whether this metabolic shift for tyramine-containing phenolamides is related to the differential nitrogen supplies between these two soils and allocation in the plant (Lou & Baldwin, 2004). We observed that putrescine and spermidine exhibit transient local responses to simulated herbivory, which precedes the biosynthesis of most abundant phenolamides such as CP and DCS. Compared with the tight regulatory control of JA- and MYB8-dependent signalling pathways over phenolamide production, which translate into massive alterations of the production of these compounds in the corresponding transgenic lines, levels of putrescine and spermidine levels were much less altered in asLOX3 and irMYB8. Such observation reinforces the idea that the control exerted by these signalling pathways for de novo phenolamides mostly occurs at the level of the phenylpropanoid pathway-dependent hydroxycinnamate flux and its branching onto polyamine metabolism.

The fact that higher constitutive phenylalanine levels were detected in sETR1 plants but not in other transgenic lines points towards a possible effect of ET on the phenylpropanoid pathway. Additional metabolic analyses would however be needed to examine possible alterations in the phenylpropanoid flux in sETR1 plants. Such a regulatory function of ET has already been suggested for the metabolism of fruits and vegetables. For instance, the ET pathway enhanced transcriptional levels of *PAL*, as well as the activity of the corresponding enzyme, during wound responses (Heredia & Cisneros-Zevallos, 2009), ripening (Villarreal, Bustamante, Civello, & Martinez, 2010) and defence responses against the fungal pathogen *Rhizopus nigricans* (Pan, Fu, Zhu, Lu, & Luo, 2013). In our study, transcript levels of *PAL2* in sETR1 did not reveal a strong effect of ET over phenolic metabolism. More generally, even though marginal reductions in elicited levels for these transcripts were observed in sETR1 compared to EV controls, these trends were not statistically significant. Of note, a previous integrative study combining transcriptomics and metabolomics analyses has shown that remodelling of BAHD gene expression and de novo phenolamide production are not strictly collinear (Woldemariam, Oh, Gaquerel, Baldwin, & Galis, 2013), suggesting that biochemical conversions among pre-existing and de novo produced phenolamides are important layers of regulation in the herbivory-elicited response. Finally, the higher levels of phenylalanine in sETR1 compared to EV plants might provide a greater source of essential amino acids to caterpillars, which could be another reason for their good performance on ET-impaired plants (Onkokesung, Baldwin, & Gális, 2010).

In conclusion, this study sheds light on the local interplay of JA-ET signalling sectors for defensive phenolamide production. Interestingly, a recent genetic repression of the circadian clock evening loop component *TOC1* in *N. attenuata* led to increase herbivory-induced levels of nicotine concomitant with lower ET signalling and strong decreases in phenolamide investments (Valim et al., 2020). Future integrative studies combining metabolome and transcriptome analyses during different types of herbivory could hence provide a clearer picture on the role of ET as one of the key orchestrators of nitrogen allocation to defence metabolite production.

ACKNOWLEDGMENTS

We are grateful to Matthias Schoettner, Michael Reichelt, Michael Stitz and Sven Heiling for technical assistance. We thank Jérôme Casas, Heidi Dalton and Dapeng Li for their valuable comments on an early version of this manuscript. The work was supported by funding from the Max Planck Society and the Collaborative Research Centre 'Chemical Mediators in Complex Biosystems—ChemBioSys' (SFB 1127) from the DFG. ENS de Lyon is thanked for its financial support to Florent Figon. Emmanuel Gaquerel's research in Strasbourg is financially supported by the CNRS and the Université de Strasbourg. Open Access funding enabled and organized by ProjektDEAL.

CONFLICT OF INTEREST

The authors declare no conflicts of interest.

ORCID

Florent Figon https://orcid.org/0000-0002-6172-3865
Ian T. Baldwin https://orcid.org/0000-0001-5371-2974
Emmanuel Gaquerel https://orcid.org/0000-0003-0796-6417

REFERENCES

Alamgir, K. M., Hojo, Y., Christeller, J. T., Fukumoto, K., Isshiki, R., Shinya, T., … Galis, I. (2016). Systematic analysis of rice (*Oryza sativa*) metabolic responses to herbivory: Defence metabolites in rice. *Plant, Cell & Environment*, *39*, 453–466.

Bassard, J.-E., Ullmann, P., Bernier, F., & Werck-Reichhart, D. (2010). Phenolamides: Bridging polyamines to the phenolic metabolism. *Phytochemistry*, *71*, 1808–1824.

Broekgaarden, C., Caarls, L., Vos, I. A., Pieterse, C. M. J., & Van Wees, S. C. M. (2015). Ethylene: Traffic controller on hormonal crossroads to defense. *Plant Physiology*, *169*, 2371–2379.

Diezel, C., von Dahl, C. C., Gaquerel, E., & Baldwin, I. T. (2009). Different lepidopteran elicitors account for cross-talk in herbivory-induced phytohormone signaling. *Plant Physiology*, *150*, 1576–1586.

Docimo, T., Reichelt, M., Schneider, B., Kai, M., Kunert, G., Gershenzon, J., & D'Auria, J. C. (2012). The first step in the biosynthesis of cocaine in *Erythroxylum coca*: The characterization of arginine and ornithine decarboxylases. *Plant Molecular Biology*, *78*, 599–615.

Erb, M., Meldau, S., & Howe, G. A. (2012). Role of phytohormones in insect-specific plant reactions. *Trends in Plant Science*, *17*, 250–259.

Gális, I., Šimek, P., Narisawa, T., Sasaki, M., Horiguchi, T., Fukuda, H., & Matsuoka, K. (2006). A novel R2R3 MYB transcription factor NtMYBJS1 is a methyl jasmonate-dependent regulator of

phenylpropanoid-conjugate biosynthesis in tobacco. *The Plant Journal*, *46*, 573–592.

Gaquerel, E., Heiling, S., Schoettner, M., Zurek, G., & Baldwin, I. T. (2010). Development and validation of a liquid chromatography–electrospray ionization–time-of-flight mass spectrometry method for induced changes in *Nicotiana attenuata* leaves during simulated herbivory. *Journal of Agricultural and Food Chemistry*, *58*, 9418–9427.

Gaquerel, E., Kotkar, H., Onkokesung, N., Galis, I., & Baldwin, I. T. (2013). Silencing an *N*-acyltransferase-like involved in lignin biosynthesis in *Nicotiana attenuata* dramatically alters herbivory-induced phenolamide metabolism. *PLoS One*, *8*, e62336.

Halitschke, R., & Baldwin, I. T. (2003). Antisense LOX expression increases herbivore performance by decreasing defense responses and inhibiting growth-related transcriptional reorganization in *Nicotiana attenuata*. *The Plant Journal*, *36*, 794–807.

Halitschke, R., Schittko, U., Pohnert, G., Boland, W., & Baldwin, I. T. (2001). Molecular interactions between the specialist herbivore *Manduca sexta* (Lepidoptera, Sphingidae) and its natural host *Nicotiana attenuata*. III. Fatty acid-amino acid conjugates in herbivore oral secretions are necessary and sufficient for herbivore-specific plant responses. *Plant Physiology*, *125*, 711–717.

Heil, M., & Baldwin, I. T. (2002). Fitness costs of induced resistance: Emerging experimental support for a slippery concept. *Trends in Plant Science*, *7*, 61–67.

Heredia, J. B., & Cisneros-Zevallos, L. (2009). The effects of exogenous ethylene and methyl jasmonate on the accumulation of phenolic antioxidants in selected whole and wounded fresh produce. *Food Chemistry*, *115*, 1500–1508.

Kallenbach, M., Alagna, F., Baldwin, I. T., & Bonaventure, G. (2010). *Nicotiana attenuata* SIPK, WIPK, NPR1, and fatty acid-amino acid conjugates participate in the induction of jasmonic acid biosynthesis by affecting early enzymatic steps in the pathway. *Plant Physiology*, *152*, 96–106.

Kang, J.-H., Wang, L., Giri, A., & Baldwin, I. T. (2006). Silencing threonine deaminase and *JAR4* in *Nicotiana attenuata* impairs jasmonic acid–isoleucine–mediated defenses against *Manduca sexta*. *The Plant Cell*, *18*, 3303–3320.

Kaur, H., Heinzel, N., Schottner, M., Baldwin, I. T., & Galis, I. (2010). R2R3-NaMYB8 regulates the accumulation of phenylpropanoid-polyamine conjugates, which are essential for local and systemic defense against insect herbivores in *Nicotiana attenuata*. *Plant Physiology*, *152*, 1731–1747.

Kim, S.-G., Yon, F., Gaquerel, E., Gulati, J., & Baldwin, I. T. (2011). Tissue specific diurnal rhythms of metabolites and their regulation during herbivore attack in a native tobacco, *Nicotiana attenuata*. *PLoS One*, *6*, e26214.

Krügel, T., Lim, M., Gase, K., Halitschke, R., & Baldwin, I. T. (2002). Agrobacterium-mediated transformation of *Nicotiana attenuata*, a model ecological expression system. *Chemoecology*, *12*, 177–183.

Kuhl, C., Tautenhahn, R., Böttcher, C., Larson, T. R., & Neumann, S. (2012). CAMERA: An integrated strategy for compound spectra extraction and annotation of liquid chromatography/mass spectrometry data sets. *Analytical Chemistry*, *84*, 283–289.

Lasanajak, Y., Minocha, R., Minocha, S. C., Goyal, R., Fatima, T., Handa, A. K., & Mattoo, A. K. (2014). Enhanced flux of substrates into polyamine biosynthesis but not ethylene in tomato fruit engineered with yeast *S*-adenosylmethionine decarboxylase gene. *Amino Acids*, *46*, 729–742.

Li, D., Halitschke, R., Baldwin, I. T., & Gaquerel, E. (2020). Information theory tests critical predictions of plant defense theory for specialized metabolism. *Science Advances*, *6*, eaaz0381.

Li, J., Zhang, K., Meng, Y., Hu, J., Ding, M., Bian, J., … Zhou, M. (2018). Jasmonic acid/ethylene signaling coordinates hydroxycinnamic acid amides biosynthesis through ORA59 transcription factor. *The Plant Journal*, *95*, 444–457.

Linke, C., Conrath, U., Jeblick, W., Betsche, T., Mahn, T., Düring, K., & Neuhaus, H. E. (2002). Inhibition of the plastidic ATP/ADP transporter protein primes potato tubers for augmented elicitation of defense responses and enhances their resistance against *Erwinia carotovora*. *Plant Physiology*, *129*, 1607–1615.

Lou, Y., & Baldwin, I. T. (2004). Nitrogen supply influences herbivore-induced direct and indirect defenses and transcriptional responses in *Nicotiana attenuata*. *Plant Physiology*, *135*, 496–506.

Marti, G., Erb, M., Boccard, J., Glauser, G., Doyen, G. R., Villard, N., … Wolfender, J.-L. (2013). Metabolomics reveals herbivore-induced metabolites of resistance and susceptibility in maize leaves and roots: Plant-insect metabolomics. *Plant, Cell & Environment*, *36*, 621–639.

Nambeesan, S., AbuQamar, S., Laluk, K., Mattoo, A. K., Mickelbart, M. V., Ferruzzi, M. G., … Handa, A. K. (2012). Polyamines attenuate ethylene-mediated defense responses to abrogate resistance to *Botrytis cinerea* in tomato. *Plant Physiology*, *158*, 1034–1045.

Onkokesung, N., Baldwin, I. T., & Gális, I. (2010). The role of jasmonic acid and ethylene crosstalk in direct defense of *Nicotiana attenuata* plants against chewing herbivores. *Plant Signaling & Behavior*, *5*, 1305–1307.

Onkokesung, N., Galis, I., von Dahl, C. C., Matsuoka, K., Saluz, H.-P., & Baldwin, I. T. (2010). Jasmonic acid and ethylene modulate local responses to wounding and simulated herbivory in *Nicotiana attenuata* leaves. *Plant Physiology*, *153*, 785–798.

Onkokesung, N., Gaquerel, E., Kotkar, H., Kaur, H., Baldwin, I. T., & Galis, I. (2011). MYB8 controls inducible phenolamide levels by activating three novel hydroxycinnamoyl-coenzyme a:polyamine transferases in *Nicotiana attenuata*. *Plant Physiology*, *158*, 389–407.

Pan, X.-Q., Fu, D.-Q., Zhu, B.-Z., Lu, C.-W., & Luo, Y.-B. (2013). Over-expression of the ethylene response factor *SlERF1* gene enhances resistance of tomato fruit to *Rhizopus nigricans*. *Postharvest Biology and Technology*, *75*, 28–36.

Paschold, A., Bonaventure, G., Kant, M. R., & Baldwin, I. T. (2008). Jasmonate perception regulates jasmonate biosynthesis and JA-Ile metabolism: The case of COI1 in *Nicotiana attenuata*. *Plant and Cell Physiology*, *49*, 1165–1175.

Schäfer, M., Brütting, C., Xu, S., Ling, Z., Steppuhn, A., Baldwin, I. T., & Schuman, M. C. (2017). NaMYB8 regulates distinct, optimally distributed herbivore defense traits. *Journal of Integrative Plant Biology*, *59*, 844–850.

Schäfer, M., Meza-Canales, I. D., Brütting, C., Baldwin, I. T., & Meldau, S. (2015). Cytokinin concentrations and CHASE-DOMAIN CONTAINING HIS KINASE 2 (NaCHK2)- and NaCHK3-mediated perception modulate herbivory-induced defense signaling and defenses in *Nicotiana attenuata*. *New Phytologist*, *207*, 645–658.

Shoji, T., Kajikawa, M., & Hashimoto, T. (2010). Clustered transcription factor genes regulate nicotine biosynthesis in tobacco. *The Plant Cell*, *22*, 3390–3409.

Smith, C. A., Want, E. J., O'Maille, G., Abagyan, R., & Siuzdak, G. (2006). XCMS: Processing mass spectrometry data for metabolite profiling using nonlinear peak alignment, matching, and identification. *Analytical Chemistry*, *78*, 779–787.

Snyder, M. J., Walding, J. K., & Feyereisen, R. (1994). Metabolic fate of the allelochemical nicotine in the tobacco hornworm *Manduca sexta*. *Insect Biochemistry and Molecular Biology*, *24*, 837–846.

Song, S., Qi, T., Wasternack, C., & Xie, D. (2014). Jasmonate signaling and crosstalk with gibberellin and ethylene. *Current Opinion in Plant Biology*, *21*, 112–119.

Stepanova, A. N., & Alonso, J. M. (2009). Ethylene signaling and response: Where different regulatory modules meet. *Current Opinion in Plant Biology*, *12*, 548–555.

Stitz, M., Gase, K., Baldwin, I. T., & Gaquerel, E. (2011). Ectopic Expression of AtJMT in nicotiana attenuata: creating a metabolic sink has tissue-specific consequences for the jasmonate metabolic network and silences downstream gene expression. *Plant Physiology*, *157*, 341–354.

Tebayashi, S., Horibata, Y., Mikagi, E., Kashiwagi, T., Mekuria, D. B., Dekebo, A., … Kim, C.-S. (2007). Induction of resistance against the

leafminer, *Liriomyza trifolii*, by jasmonic acid in sweet pepper. *Bioscience, Biotechnology, and Biochemistry*, *71*, 1521–1526.

Ullmann-Zeunert, L., Stanton, M. A., Wielsch, N., Bartram, S., Hummert, C., Svatoš, A., … Groten, K. (2013). Quantification of growth-defense trade-offs in a common currency: Nitrogen required for phenolamide biosynthesis is not derived from ribulose-1,5-bisphosphate carboxylase/oxygenase turnover. *The Plant Journal*, *75*, 417–429.

Valim, H., Dalton, H., Joo, Y., McGale, E., Halitschke, R., Gaquerel, E., … Schuman, M. C. (2020). *TOC1* in *Nicotiana attenuata* regulates efficient allocation of nitrogen to defense metabolites under herbivory stress. *New Phytologist*, *228*, 1227–1242.

Villarreal, N. M., Bustamante, C. A., Civello, P. M., & Martinez, G. A. (2010). Effect of ethylene and 1-MCP treatments on strawberry fruit ripening. *Journal of the Science of Food and Agriculture*, *90*, 683–689.

von Dahl, C. C., Winz, R. A., Halitschke, R., Kühnemann, F., Gase, K., & Baldwin, I. T. (2007). Tuning the herbivore-induced ethylene burst: The role of transcript accumulation and ethylene perception in *Nicotiana attenuata*. *The Plant Journal*, *51*, 293–307.

Wang, K. L.-C., Li, H., & Ecker, J. R. (2002). Ethylene biosynthesis and signaling networks. *The Plant Cell Online*, *14*, S131–S151.

Wang, L., & Wu, J. (2013). The essential role of jasmonic acid in plant–herbivore interactions – Using the wild tobacco *Nicotiana attenuata* as a model. *Journal of Genetics and Genomics*, *40*, 597–606.

Wang, W., Yu, Z., Meng, J., Zhou, P., Luo, T., Zhang, J., … Lou, Y. (2020). Rice phenolamindes reduce the survival of female adults of the white-backed planthopper *Sogatella furcifera*. *Scientific Reports*, *10*, 5778.

Wasternack, C., & Hause, B. (2013). Jasmonates: Biosynthesis, perception, signal transduction and action in plant stress response, growth and development. An update to the 2007 review in Annals of Botany. *Annals of Botany*, *111*, 1021–1058.

Winz, R. A., & Baldwin, I. T. (2001). Molecular interactions between the specialist herbivore *Manduca sexta* (Lepidoptera, Sphingidae) and its natural host *Nicotiana attenuata*. IV. Insect-induced ethylene reduces jasmonate-induced nicotine accumulation by regulating *putrescine N*-methyltransferase transcripts. *Plant Physiology*, *125*, 2189–2202.

Woldemariam, M. G., Oh, Y., Gaquerel, E., Baldwin, I. T., & Galis, I. (2013). NaMYC2 transcription factor regulates a subset of plant defense responses in *Nicotiana attenuata*. *BMC Plant Biology*, *13*, 73.

Wu, J., Hettenhausen, C., Meldau, S., & Baldwin, I. T. (2007). Herbivory rapidly activates MAPK signaling in attacked and unattacked leaf regions but not between leaves of *Nicotiana attenuata*. *The Plant Cell*, *19*, 1096–1122.

Wuddineh, W., Minocha, R., & Minocha, S. C. (2018). Polyamines in the context of metabolic networks. In R. Alcázar & A. F. Tiburcio (Eds.), *Polyamines* (pp. 1–23). New York, NY: Springer.

SUPPORTING INFORMATION

Additional supporting information may be found online in the Supporting Information section at the end of this article.

How to cite this article: Figon F, Baldwin IT, Gaquerel E. Ethylene is a local modulator of jasmonate-dependent phenolamide accumulation during *Manduca sexta* herbivory in *Nicotiana attenuata*. *Plant Cell Environ*. 2021;44:964–981. https://doi.org/10.1111/pce.13955